DEVELOPMENT OF HARDWARE FOR IMPEDANCE CARDIOGRAPHY

A dissertation
submitted in partial fulfillment of the requirements
for the degree of

Master of Technology

by

L. Venkatachalam

(Roll No. 04330402)

under the supervision of

Prof. P. C. Pandey

Biomedical Engineering Group
School of Biosciences and Bioengineering
Indian Institute of Technology, Bombay
July 2006

L. Venkatachalam / Prof. P. C. Pandey (supervisor): “Development of hardware for impedance cardiography”, *M.Tech. dissertation*, Biomedical Engineering Group, School of Biosciences and Bioengineering, Indian Institute of Technology, Bombay, June 2006.

ABSTRACT

Impedance cardiography is a non-invasive technique for measuring cardiac output and for diagnosing cardiac disorders. The basal impedance of human thorax is normally $20 – 30\ \Omega$ and it decreases by $0.1 – 0.2\ \Omega$ during systole due to blood pumped into the thoracic region. This change in the thoracic impedance is sensed by injecting a high frequency (20 – 100 kHz) current (<5 mA) into the thoracic region through a pair of electrodes and by measuring the voltage across another pair of electrodes. The impedance variation thus measured is known as impedance cardiogram (ICG) and can be used for estimating stroke volume by using appropriate models of blood flow and can also be used for diagnostic information. The objective is to improve the hardware modules of the existing instrument for better performance. The oscillator module has been modified for better short term amplitude stability. The precision rectifier in the demodulator has been modified for better frequency response. The parameters of the drift cancellation circuit has been modified for better performance. An earlier microcontroller based designed thoracic impedance simulator has been enhanced by using a digital potentiometer based circuit, to simulate step and sinusoidal types of variation in change in the impedance, for testing and calibration of impedance cardiograph.

ACKNOWLEDGEMENTS

I would like to express my deepest gratitude to my guide Prof. P. C. Pandey for his guidance, support, and encouragement throughout the course of this project. I am also thankful to Prof. S. Mukherji and Prof. L. R. Subramanyan for their invaluable comments and suggestions.

I am thankful to my colleges in SPI lab Mr. Vinod K. Pandey, Mr. Jignesh N. Sarvaiya, Mr. A. R. Jayan, and my friends Mr. M. Suresh, Mr. V. Vinod Kumar, and Mr. Vikas K. Patel for their helpful suggestions and the useful discussions I had with them. I would also like to thank my lab members Mr. Priyanko Mitra and Mr. Gidda Reddy Gangula for their help in software programming part.

I would also like to thank Mr. Dinesh Choudhary and Mr. Vidyadhar Kamble for their suggestions and help in making PCB layouts for this project.

L. Venkatachalam

July 2006

CONTENTS

LIST OF SYMBOLS

Symbol	Explanation
ΔV	Volume change of the small parallel column
ρ	Resistivity of the material in the small parallel column
L	Length of the column
Z_o	Impedance of the fixed conduction volume
ΔZ	Impedance change across the column
$-(dz/dt)_{\max}$	Most negative (upward in the graph) deflection during systole measured from zero.
T_{lvet}	Left ventricle ejection time
Z_n	Impedance of changing volume
$z(t)$	Impedance cardiogram
dZ/dt	Differentiated impedance cardiogram

LIST OF ABBREVIATIONS

Symbol	Explanation
ICG	Impedance cardiogram
ECG	Electrocardiogram
PCG	Phono cardiogram
CO	Cardiac output
SV	Stroke volume
ADC	Analog-to-digital converter
DAC	Digital-to-analog converter
PWM	Pulse width modulation
DC	Direct current
SAR	Successive approximation register
SNR	Signal-to-noise ratio
PCB	Printed circuit board
CM	Common mode
DM	Differential mode
CMRR	Common mode rejection ratio

LIST OF FIGURES

LIST OF TABLES

Chapter 1
INTRODUCTION

1.1 Background

The electrical activity of the heart can be monitored by investigating the electrocardiogram (ECG). But the main action of the heart is mechanical pumping of blood. Impedance cardiography (ICG) is a technique which allows non-invasive monitoring of this mechanical action of the heart. It involves injecting a high frequency low intensity current into the thorax through a pair of electrodes. Voltage developed across a pair of sensing electrodes gets amplitude modulated because of variation in the thoracic impedance due to changing blood volume. The variation in the impedance is sensed and used for estimating the stroke volume (SV) i.e., the amount of blood pumped by the heart per heartbeat and for obtaining other diagnostic information on cardiac functioning. Compared to other techniques, ICG is non-invasive, easy to apply and low in cost.

1.2 Project objective

This project involves modification of the hardware used for the existing impedance cardiograph instrument developed at IIT Bombay for better performance. It is a continuation of earlier work done at IIT Bombay. The instrument consists of an oscillator, a V-I converter for current excitation of the thorax, voltage sense amplifier, demodulator and drift cancellation circuit. The sections which need to be modified include the oscillator section whose short term amplitude stability needs to be improved, the V-I converter in which the stray current and common mode pick-ups has to be reduced, the instrumentation amplifier whose CMRR can be increased and the demodulator section where the performance at the frequency used (100 kHz) is not satisfactory and the modification of the parameters of the drift cancellation circuit for optimum use of the ADC dynamic input range.

A thorax simulator is required for testing and calibration of impedance cardiograph. This has been developed as an upgradation of an microcontroller based earlier design, with provision for variation of heart rate, basal impedance, change in impedance, shape of change in impedance (square or sine) and amplitude of ECG common mode and differential mode signals.

1.3 Dissertation outline

Chapter 2 reviews the basics of impedance cardiography. The third chapter gives the block description of the existing instrument. The hardware modifications implemented in the impedance cardiograph instrument are reported in the fourth chapter. The fifth chapter gives details about the design of the thorax simulator. The sixth chapter gives a summary of the work and some suggestions for future work.

Chapter 2
BASICS OF IMPEDANCE CARDIOGRAPHY

2.1 Anatomy of the heart

The heart consists of four chambers namely left atrium, left ventricle, right atrium, and right ventricle, as shown in Fig. 2.1 [1][2][3]. The left atrium and ventricle are separated by the mitral valve. The right atrium and right ventricle are separated by the tricuspid valve. The valves between the atrium and the ventricle are also known as atrio-ventricular (A-V) valves. The pulmonic valve is situated between the right ventricle and the pulmonary artery and the aortic valve between the left ventricle and the aorta. The deoxygenated blood (blood poor in oxygen content) from all peripheral organs of the body flow into the right atrium. The right atrium pumps it to the right ventricle, from where it is pumped to the lungs through pulmonary arteries for oxygenation. From the lungs, the blood arrives to the left atrium through pulmonary veins. The left atrium pumps the oxygenated blood to the left ventricle which in turn pumps it to the peripheral organs through the aorta, completing the blood circulation. The mechanical activity of the heart is actually caused by the electrical activity of the cardiac muscle cells. Each cycle is initiated by spontaneous generation of an action potential in the sino-atrial (SA) node located in the anterior wall of the right atrium. These potentials travel through both atrium to the A-V node, located between the atriam and ventricles, and then to the ventricles.

2.2 The cardiac cycle

A cardiac cycle consists of a systole and diastole of both atria plus a systole and diastole of both ventricles. As a chamber of the heart contracts, the pressure of the fluid within it increases. Due to this, pressure changes occur and blood flows from areas of higher blood pressure to areas of lower blood pressure. As shown in Fig. 2.2.

the cardiac cycle can be divided into three phases: diastole or relaxation, ventricular filling, and ventricular systole.

In the relaxation phase, all four chambers are in diastole at the end of a heartbeat. As the ventricles relax, pressure within the chambers drops and blood starts to flow from the pulmonary trunk and aorta back towards the ventricles. As the pressure drops below the aortic pressure, the aortic valves close. There is a brief interval when the ventricular blood volume does not change because both A-V valves and aortic and pulmonic valves are closed. This period is called isovolumic relaxation. As the ventricles relax, the space inside expands and the pressure falls rapidly. When ventricular pressure falls below atrial pressure, the A-V valves open and ventricular filling begins.

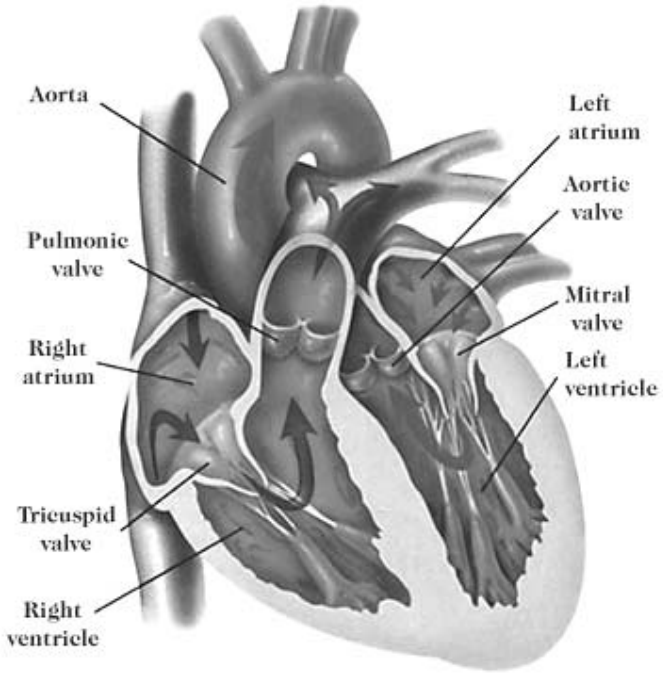

Fig. 2.1 The chambers of the heart and blood vessels [3]

As soon as the A-V valves open, there is a large amount of blood flow which had accumulated in the atria during the time the ventricles were contracting. The firing of the SA node results in atrial depolarization which is followed by atrial contraction after some time. At the end of ventricular diastole, there is about 130 ml of blood in each ventricle which is known as end-diastolic volume (EDV).

The impulse from the SA node after passing through the A-V node reaches the ventricles causing them to depolarize. Ventricular contraction begins and blood is pushed up against the A-V valves forcing them shut. As ventricular contraction continues, the pressure inside rises rapidly. For about 0.05 s, all four valves are closed again. This period is called isovolumic contraction. When left ventricular pressure surpasses aortic pressure and right ventricular pressure rises above the pressure in the pulmonary trunk, both aortic and pulmonic valves open and ejection of blood begins and continues until the ventricles start to relax. Then the aortic and pulmonic valves close and another relaxation period begins. The volume of blood still left in each ventricle after ventricular systole is known as end-systolic volume (ESV). At rest, it is about 60 ml.

During each cardiac cycle, four heart sounds are generated. In a normal heart, however, only the first two are loud enough to be heard by stethoscope. The first heart sound, which can be described as "lubb", is the sound created by blood turbulence associated with closure of the A-V valves soon after ventricular systole begins. The second heart sound, which can be described as "dub", is the sound created by blood turbulence associated with closure of the aortic and pulmonic valves at the beginning of ventricular diastole.

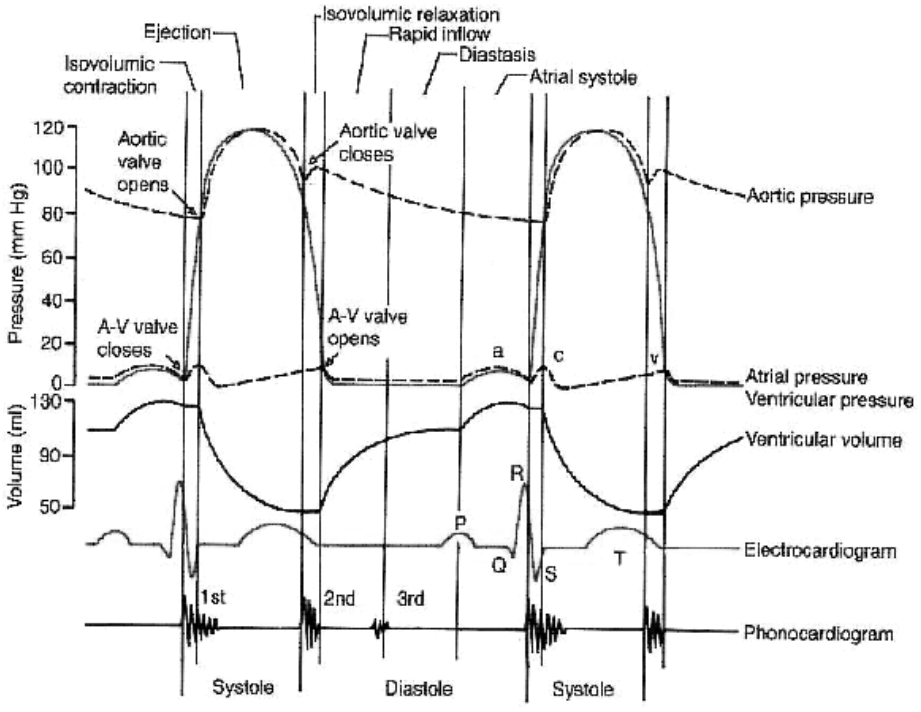

Fig. 2.2 The cardiac cycle [1]

2.3 Cardiac output

The volume of blood ejected by the ventricle with each contraction is known as stroke volume (SV). Cardiac output (CO) is the amount of blood ejected from the left ventricle (or the right ventricle) into the aorta (or pulmonary trunk) each minute. Thus, cardiac output is SV times the heart rate (HR), the number of heartbeats per minute. In a typical resting adult, the stroke volume averages 70 ml/beat and heart rate is about 72 beats/min. This gives an average CO of 5.04 litres/min.

Stroke volume is the difference between the end-diastolic volume (EDV) and end-systolic volume (ESV). Three important factors regulate stroke volume in different circumstances: preload, contractility and afterload [1][2].

Preload: This refers to the amount of stretch on cardiac muscle fibres just before they contract. According to Frank-Starling law of the heart [1], the more the heart is filled during diastole, the greater the force of contraction during systole i.e., the greater the EDV, the more forceful the contraction. EDV is determined by two factors: duration of ventricular diastole and venous pressure. When heart rate increases, the duration of diastole is shorter. Less filling time means a smaller EDV and the ventricles may contract before they are adequately filled. When the venous pressure increases, the amount of blood forced into the ventricles increases and EDV increases.

Contractility: This is the strength of contraction of the ventricular muscles at any given preload. Substances that increase contractility are called positive inotropic agents and those that decrease contractility are called negative inotropic agents. Thus, for a given preload, the stroke volume is larger when a positive inotropic substance is present. Positive inotropic agents promote Ca^{2+} inflow during cardiac action potentials which strengthens the force of the subsequent muscle fibre contraction. They include stimulation of the sympathetic division of the autonomic nervous system, hormones such as epinephrine and norepinephrine, increased Ca^{2+} level in the extracellular fluid, and the drug digitalis. Negative inotropic agents include inhibition of the sympathetic division of the autonomic nervous system, anoxia, acidosis, some anesthetics, and increased K^{+} level in the extracellular fluid.

Afterload: This refers to the pressure that must be exceeded before ejection of blood from the ventricles can begin i.e., the pressure that must be overcome before the semilunar valves can open. When afterload increases, the stroke volume decreases.

Afterload can increase when blood pressure is elevated or arteries are narrowed by atherosclerosis.

2.4 Basis for impedance cardiography

The resistivity of blood is lesser than that of other body tissues [4][5]. Thus, when the volume of blood in the thoracic cavity increases, the impedance of the thorax decreases. The typical values of resistivity of biological materials [4] are given in Table 2.1.

Table 2.1 Resistivity of biological materials [4]

Material	**Resistivity (ρ), Ω.cm**
Blood	150
Plasma	63
Cardiac muscle	750
Lung	1275
Fat	2500

In impedance cardiography, a high frequency (20 – 400 kHz) low amplitude (<5 mA) current is passed through the thorax [4][5]. During systole, when the volume of blood in the thorax increases, the impedance falls. The corresponding voltage drop is recorded which is thus proportional to the stroke volume. The mean impedance of the thorax is about 20 Ω and change in impedance is 0.1 to 0.2 Ω [5][6].

An impedance model for the thorax was proposed by Kubicek and a formula for stroke volume calculation was derived by him from the model [7][8]. The model known as parallel column model consists of two parallel columns of conducting material as shown in Fig. 2.3, one with constant impedance Z_o and other with a variable impedance Z_N. The net impedance is given by

$$Z(t) = Z_o \parallel Z_N \qquad (2.1)$$

If the cross sectional area of the column "N" varies from zero to a finite value the change in impedance across the parallel column is given by

$$z(t) = Z(t) - Z_o$$

and hence

$$z(t) = -\frac{Z_o^{\,2}}{(Z_o + Z_N)} \tag{2.2}$$

Since $Z_N >> Z_o$, we can write

$$z(t) \approx -\frac{Z_o^{\,2}}{Z_N} \tag{2.3}$$

If the excitation frequency used for impedance measurement is kept in 40 – 400 kHz, the impedance measured is almost nearly resistive. Hence impedance terms used in this discussion actually refers to resistance.

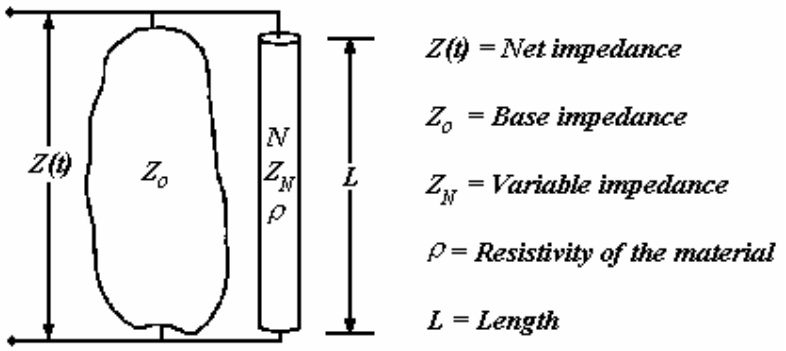

Fig. 2.3 Parallel column model [9]

Considering Z_N to be a cylinder with length, *L*, cross-sectional area, *A*, and volume $v = LA$, Z_N is given by

$$Z_N = \frac{\rho L^2}{v} \tag{2.4}$$

where, ρ is the resistivity of the material. Hence the impedance variation can be given as

$$z(t) = -\frac{Z_o^{\,2} v}{\rho L^2} \tag{2.5}$$

An assumption was made that the inflow of blood into the thorax is the source of impedance change and the volume of the column N is zero before systole. So during systole, the impedance starts decreasing and assuming no blood leaves the thorax during systole, the maximum impedance change can be written as

$$\Delta Z = (-z)_{\max}$$

The change in volume of the column, $\Delta V = V_{max}$ is given by

$$\Delta V = \rho \frac{L^2}{Z_o^{\,2}} \Delta Z \tag{2.6}$$

The outflow of blood from the lungs into the heart was not accounted during systole. Later a correction was made [7][8], in which the extrapolation technique shown in Fig. 2.4, was introduced to account for the outflow of blood from the lungs into the heart in the later part of systole. This is as given below

$$\Delta V = \frac{\rho L^2}{Z_o^{\,2}} \left(-\frac{dz}{dt} \right)_{\max} T_{lvet} \tag{2.7}$$

where, $\left(-\frac{dz}{dt} \right)_{\max}$ is the most negative (upward in the graph) deflection during systole measured from zero, and T_{lvet} is the left ventricular ejection time (time between the first heart sound "B" and aortic valve closure "X") as shown in Fig. 2.4. A number of other refinements have been reported [9][10].

2.5 Impedance cardiogram

The impedance variation signal is *z(t)* waveform. It is customary to plot -*z*(*t*), because an increase (positive deflection) in this waveform is related to increase in the volume of blood. The derivative of this waveform, -*dz*/*dt* is termed as the impedance cardiogram, and is used for calculation of stroke volume, as well as for obtaining diagnostic information. A typical impedance cardiogram is shown in Fig. 2.5. The 'R' point of the ECG waveform is used as a reference. Phonocardiogram (PCG) is used as a reference to monitor the heart sounds resulting from opening and closing of heart valves. Points on the *dz/dt* waveform have been identified to correspond to the following physiological events:

A: Atrial contraction
B: Closure of tricuspid valve
X: Closure of aortic valve
Y: Closure of pulmonic valve
O: Opening snap of mitral valve
Z: Third heart sound

The contribution of cardiovascular system to the impedance signal is a sum of two components [9]:

1. Plethysmographic component – The contraction of the ventricles causes the pressure in aorta to change which in turn causes the volume of the aorta to change leading to the impedance change.

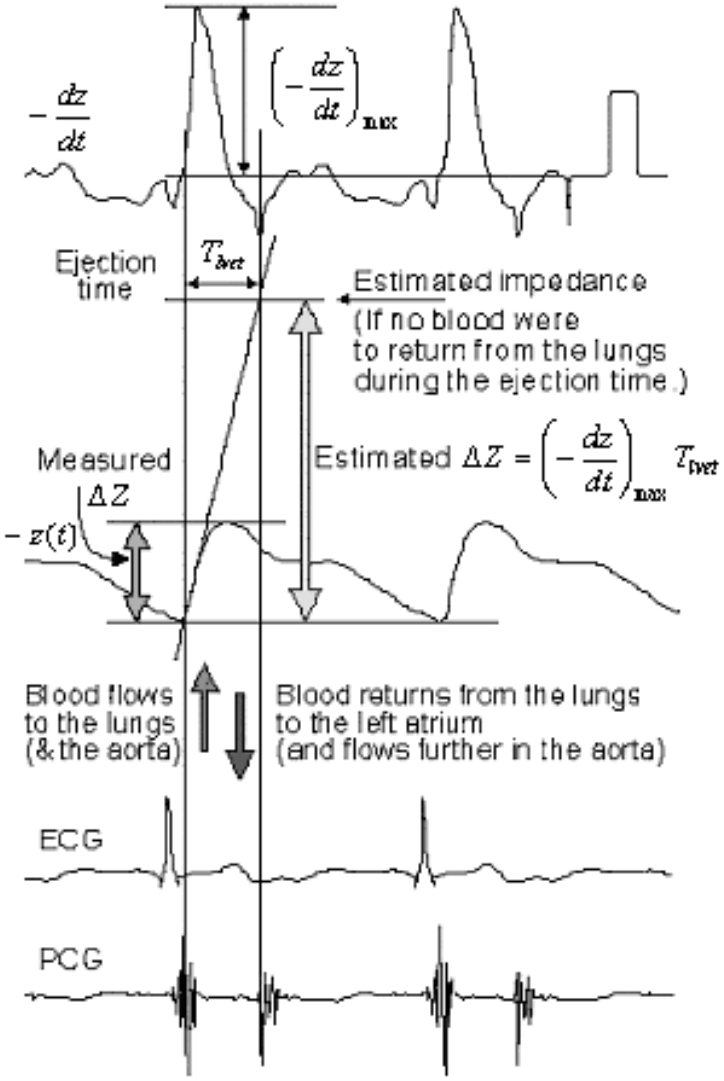

Fig. 2.4 Stroke volume calculation by extrapolation technique [7]

2. Erythrocyte-orientation component – At the end of diastole, the erythrocytes are randomly oriented within the plasma. The current lines have an extended path-length and the resistivity of blood is high. During systole, the erythrocytes become aligned with their plane parallel to the main axis of the aorta. As the velocity increases, the percentage of aligned erythrocytes

increases thus, the conductivity of flowing blood is higher than that of stationary blood.

The heart itself does not significantly contribute to the impedance signal due to the following reasons:

1. The physical volume of the heart represents 10% of the total volume of the thorax and its conductivity is totally shielded by the aorta and the vena cava.
2. During systole, the heart is expelling blood increasing its impedance while the impedance of the blood vessels is decreasing due to the inflow of blood into them.

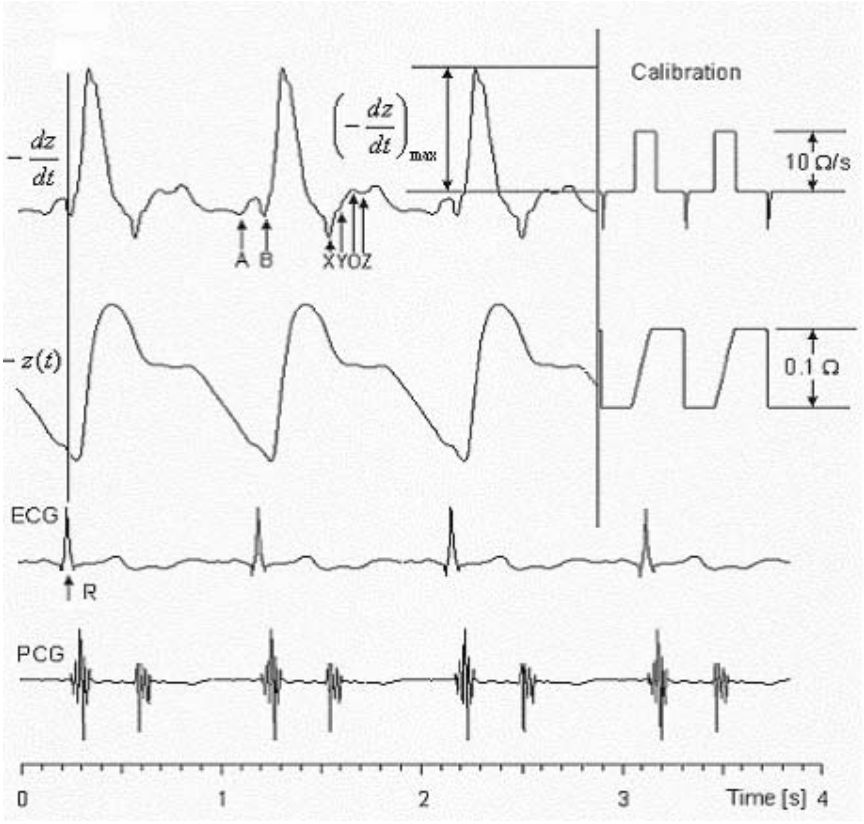

Fig. 2.5 Typical impedance cardiography related waveforms -*z*(*t*) and -*dz*/*dt*, along with ECG and PCG [7]

2.6 Earlier work at IIT Bombay

Work on impedance cardiography has been carried out at IIT Bombay from 1990 onwards. An instrument for measuring the cardiac output and stroke volume was developed by Joshi in 1993 [11][12]. In 1997, Patwardhan developed software for off-line display of all the recorded physiological signals and also developed a thorax simulator for calibration of the impedance cardiograph [13]. Kuriakose in 2000

modified the circuit to improve the sensitivity and consistency of the instrument [14]. Manigandan in 2004 improved the instrument further, particularly by implementing a microcontroller based drift cancellation circuit and improving the thorax simulator [15]. Later Naidu in 2005 improved the short term amplitude stability of the oscillator, implemented vector lock-in amplifier technique for demodulator, modified the parameters of the drift cancellation circuit for optimum use of the ADC dynamic input range and developed a microcontroller based impedance simulator [16]. During the same period, work has been carried out by Vinod K. Pandey on improving the signal processing of ICG waveform [17][18].

Chapter 3

IMPEDANCE CARDIOGRAPH

3.1 Block diagram

As a result of earlier work at IIT Bombay [13][14][15][16] based on the design used by Qu *et al.* [19][20], a prototype ICG instrument was developed. The block diagram of the instrument is as shown in Fig. 3.1. The various blocks are explained below.

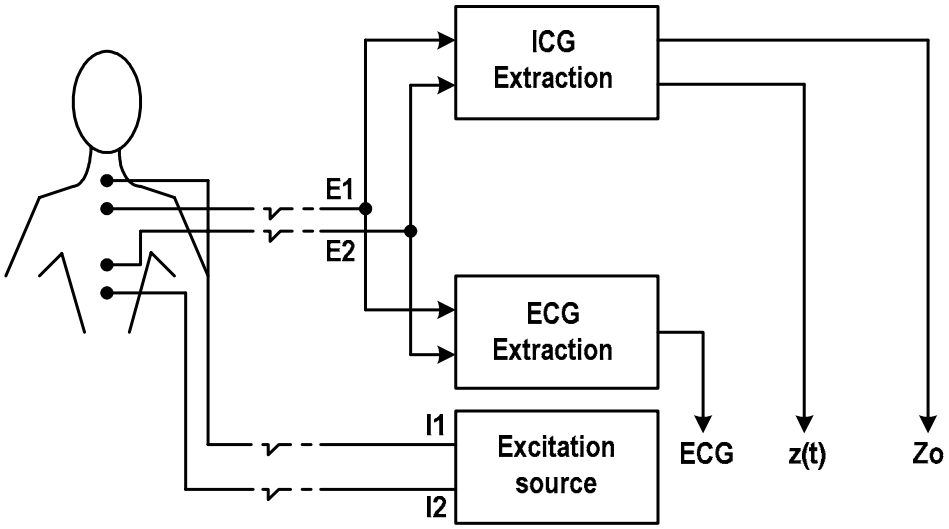

Fig. 3.1 Block diagram of the existing ICG instrument [15]

3.1.1 Excitation circuit

A Wein bridge oscillator and a voltage-to-current converter constitute the excitation circuit. The Wein bridge oscillator produces a sinusoidal waveform of 100 kHz. There is a buffer stage to improve stability of the oscillator by avoiding the load on the oscillator. Two circuits were tested for the voltage-to-current converter: unbalanced and balanced. In the unbalanced one, one of the current injection points is at virtual ground and the output voltage is developed at the other end. In the balanced one, the two current injection points are maintained at 180° phase [21][22]. In the assembled prototype, the unbalanced voltage-to-current converter was used.

3.1.2 ICG and ECG extraction circuits

The two voltage sensing electrodes are connected to the ICG extraction circuit. It consists of an instrumentation amplifier with bandpass filter, demodulator, averager for Z_o and drift cancellation circuit for $z(t)$. The instrumentation amplifier amplifies the signal obtained and has a 16 kHz high pass filter at the input to attenuate power line and other low frequency pickups, ECG, and other motion artifacts, without affecting the signal centered around 100 kHz. The demodulator section consists of a full wave precision rectifier followed by a low pass filter to get the impedance waveform. A microcontroller based drift cancellation circuit is used to remove respiration artifacts to obtain $z(t)$. The pair of voltage sensing electrodes is also connected to ECG extraction circuit which has an instrumentation amplifier and a low pass filter to get ECG. The ECG is obtained from two sensing electrodes on the chest and is different from the signals obtained using standard leads. The ECG is primarily for use as timing reference for processing of the ICG waveform, and not meant for any diagnostic information itself. Provision for obtaining ECG from limb electrode configuration has also been provided. High impedance indicator circuit indicates whether the contacts of the electrodes with the body are proper or not.

3.2 Software signal processing

The signals, $z(t)$, Z_o, ECG, and PCG are acquired using a USB-based data acquisition unit. The PCG signal is obtained from a separate phonocardiograph. The signals are processed using filters, the required parameters according to the formula for SV are evaluated and the SV calculated. The signal processing is done in MATLAB. Most of the motion artifacts fall in the range of the frequency range of $z(t)$ and thus filtering can not be done to remove them. In this case, ensemble averaging can be used with the R points of the ECG waveform providing as fiducial marks [17].

3.3 Electrodes

There are two possible kinds of electrode configurations possible: two-electrode and four-electrode. A four-electrode configuration of electrodes is used, wherein; two outer electrodes inject current while two inner electrodes detect the voltage. In a two- electrode configuration, the two electrodes injecting current also measure the voltage. This can lead to errors because of voltage drops across the skin-electrode contact impedance [23]. This is eliminated in a four electrode configuration. Suction

cup stainless steel electrodes are used for the current injecting electrodes and pre-gelled disposable Ag-AgCl ECG electrodes are used as the sensing electrodes. Gel is applied between the electrode and the skin at the skin-electrode interface to obtain a good contact. The instrument can also be used with band electrodes.

The main sources of interference in ICG are from respiration and body movements. Respiration causes changes in the amount of air in the thorax and movement of the thorax which leads to changes in the impedance. The changes in the orientations and locations of the internal body parts during movements also contribute to noise by changing the distribution of current in the body segment. Electrodes are placed in the central area of the body where body movements cause minimal displacement of the electrodes. They are also located in the area which is the largest contributor to the impedance signal.

3.4 Hardware modifications needed

The short term amplitude instability of the oscillator has to be studied and brought down. The precision rectifier used for amplitude demodulation does not perform well at the excitation frequency used (100 kHz). Therefore this section needs to be modified by changing the configuration in the existing circuit or by going in for a different demodulation scheme. The drift cancellation circuit has to be modified for optimum use of the ADC dynamic input range.

Chapter 4
THORAX SIMULATOR

4.1 Introduction

A thorax simulator is necessary for testing and calibration of the impedance cardiograph instrument and has been developed based on earlier designs [15][16]. The unit developed can be used for testing and calibration of (a) the ICG extraction circuit, or (b) the ECG extraction circuit. It generates sinusoidal and step changes in resistance which can be used for finding the sensitivity and response time (or bandwidth) of the impedance detector circuit of the instrument. It generates square pulses of known magnitude, both in differential mode as well as common mode for testing the gain and CMRR of the ECG amplifier circuit of the instrument. It has been designed to work in only one of these modes at a time. Option for feeding external pick-ups is also incorporated. The simulator is powered by a 9 V battery. An earlier design by Manigandan [15] used astable multivibrators, manual switches, and potentiometers. In order to reduce wiring related pick-ups and to introduce flexibility in operation, Naidu [16] redesigned the unit with a microcontroller and analog switches based circuit which takes inputs from two input keys for selection of various options and has a LCD for display. The earlier designs were capable of simulating only step change in impedance. In the new design, a digital potentiometer replaces the analog switches used to generate impedance variations. The digital potentiometer in the new design facilitates to simulate step, sinusoidal or other types of variation in change in the impedance.

4.2 Thorax simulator model

A resistive model of the thorax, used in the thorax simulator is shown in Fig. 4.1. The high frequency current is injected through the terminals corresponding to the current electrodes I1 and I2. The variation in impedance is sensed through the

terminals E1 and E2, corresponding to the voltage sensing electrodes. In this model, R_e's constitute the tissue-electrode contact resistances for 4-electrode configuration. Resistances R_o and R_s are the parallel column model resistances and R_{s1} and R_{s2} are the fixed resistances in the current path. Option for feeding external pick-up is denoted by V_p and the resistance in the pick-up path by R_p. The voltage sources V_{ed} and V_{ec} represent the differential mode and common mode ECG signals respectively.

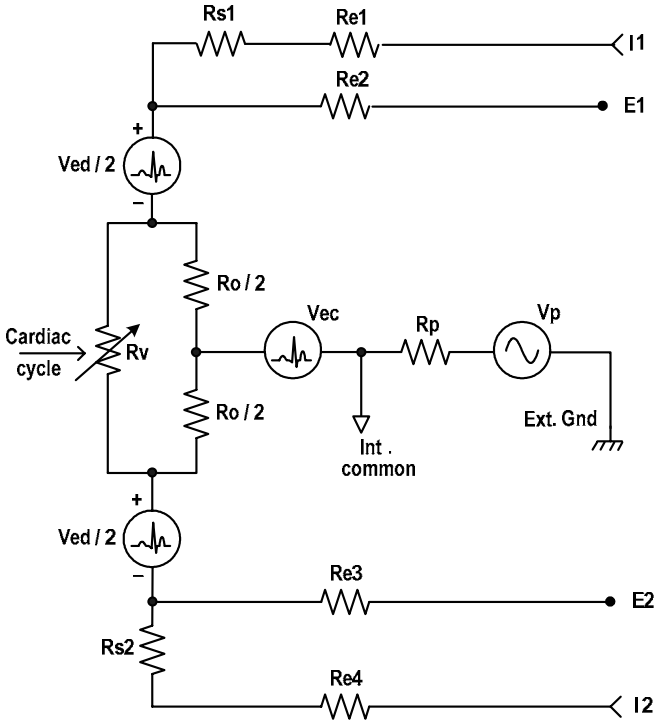

Fig. 4.1 Thorax model

A very simplified simulation of the variation in the thoracic impedance is used here. The thoracic resistance is given as $R_s \parallel R_v$, with R_v varying with cardiac systole pulses. This pulsating change in the resistance is useful for calibration of the impedance detector circuit of the ICG instrument. Voltages V_{ed} and V_{ec} can be used for calibration and testing of the ECG amplifier circuit of the instrument. Further if the model is implemented, such that we either have resistance variations or the ECG voltages, the sensitivity of the two circuits and their cross-responses can be tested. Externally injected voltage V_p can be used for testing the pickup rejection by both circuits of the instrument.

4.3 Simulator circuit

The thorax model of Fig. 4.1 has several sources without a common node. In order to have an easily realizable circuit, the model can be modified to a schematic shown in Fig. 4.2. Relations of the component values in the schematic of Fig. 4.2 to those in the model of Fig. 4.1 are as the following

$$R_1 = R_{s1} + R_{e1} \tag{4.1}$$

$$R_2 = R_{e2} \tag{4.2}$$

$$R_3 = R_{e3} \tag{4.3}$$

$$R_4 = R_{e4} + R_{s2} \tag{4.4}$$

$$R_O = R_Z \,\|\, (R_{y1} + R_{y2}) \,\|\, (R_{x1} + R_{x2}) \tag{4.5}$$

The differential (DM) and common mode (CM) voltages are developed by two square wave voltages V_{x1} and V_{x2} which develop the voltages V_1 and V_2 at points A and B respectively.

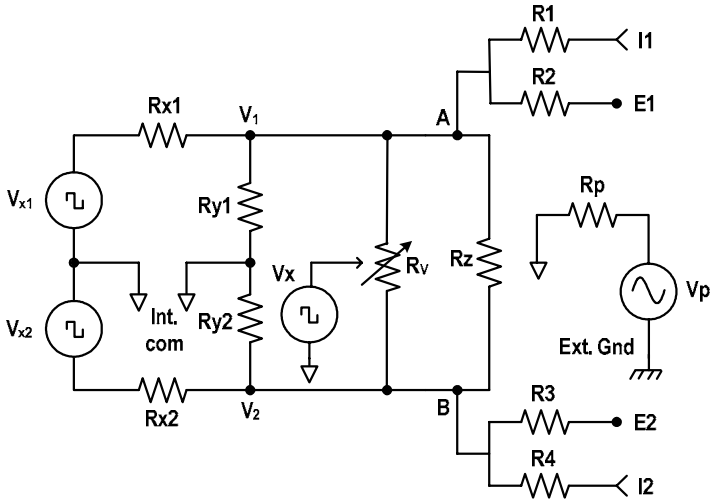

Fig. 4.2 Schematic of the model shown in Fig. 4.1

The voltages V_{ed} and V_{ec} of Fig. 4.1 are related to voltages $V_1$and V_2 of Fig. 4.2 by

$$V_{ed} = V_1 - V_2 \tag{4.6}$$

$$V_{ec} = 0.5(V_1 + V_2) \tag{4.7}$$

In Fig. 4.2, we have

$$V_1 = V_{x1} \times R_{y1}' / (R_{x1} + R_{y1}') \tag{4.8}$$

$$V_2 = V_{x2} \times R_{y2}' / (R_{x2} + R_{y2}') \quad (4.9)$$

where,

$$R_{y1}' = R_{y1} \parallel \left(R_z + \left(R_{y2} \parallel R_{x2}\right)\right),$$
$$R_{y2}' = R_{y2} \parallel \left(R_z + \left(R_{y1} \parallel R_{x1}\right)\right)$$

Thus by controlling V_{x1} and V_{x2} we can vary V_{ed} and V_{ec}.

4.4 Hardware blocks of the simulator

The impedance simulator consists of four blocks: (i) variable resistance circuit, (ii) CM/DM ECG simulator, (iii) digital controller, (iv) power supply. These blocks are described in the following subsections.

4.4.1 Variable resistance circuit

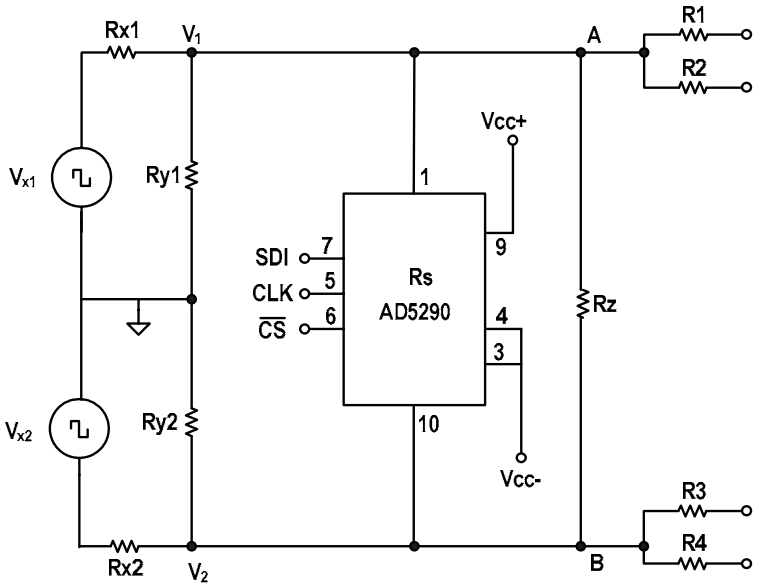

Fig. 4.3 Circuit diagram of resistance simulator

The circuit diagram of the variable resistance circuit for the schematic shown in Fig. 4.2 is shown in Fig. 4.3. The resistance across points AB is given as

$$R_{eq} = R_z \,||\, R_V \,||\, ((R_{x1} \,||\, R_{y1}) + (R_{x2} \,||\, R_{y2})) \quad (4.10)$$

The variable resistance R_V provided by the digital potentiometer is given as

$$R_V = R_{V(max)} \times n / 255 \quad (4.11)$$

where $0 \leq n \geq 255$ is the control byte written to the digital potentiometer for controlling its resistance. Different base values of *Rz* can be realized by using resistances in series with analog switches. For this purpose, CD4066 with quad analog switches has been used. All the 4 switches in an IC are connected in parallel together to reduce the on-resistance, and the effective variation in on-resistance. Circuit diagram of the four values of *Rz* are governed by control voltages RB7 and RB6, and are given as

$$(R_z)_{00} = R_{28} + R_{29}$$

$$(R_z)_{01} = (R_{28} + R_{29}) \,||\, (R_{32} + R_{s9(on)} + R_{33})$$

$$(R_z)_{10} = (R_{28} + R_{29}) \,||\, (R_{30} + R_{s8(on)} + R_{31})$$

$$(R_z)_{11} = (R_{28} + R_{29}) \,||\, (R_{30} + R_{s8(on)} + R_{31}) \,||\, (R_{32} + R_{s9(on)} + R_{33})$$

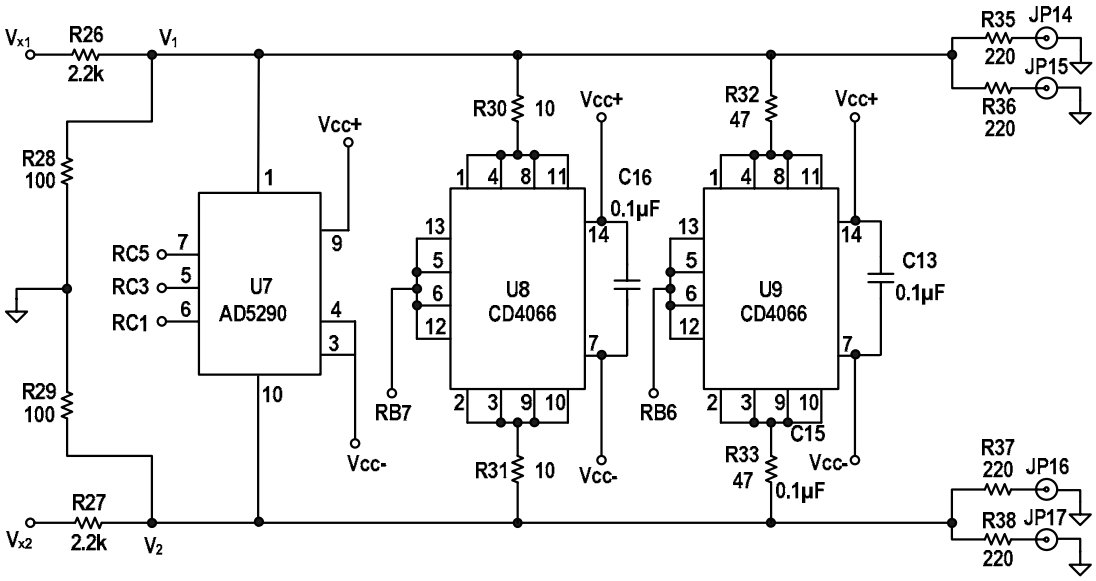

Fig. 4.4 Circuit diagram of thoracic resistance simulator with multi-basal thoracic resistances

4.4.2 Power supply

The power supply circuit generates +5 V and ground for the digital section and +2.5 V, -2.5 V and ground for the analog section, from a single 9 V supply as shown in Fig. 4.5. It consists of two voltage regulators, U1 and U2, which give +5 V at their output. An opamp (U3A) is used to generate the midpoint of the supply which is used as analog ground for the circuit and with respect to this ground, we get ±2.5 V supply.

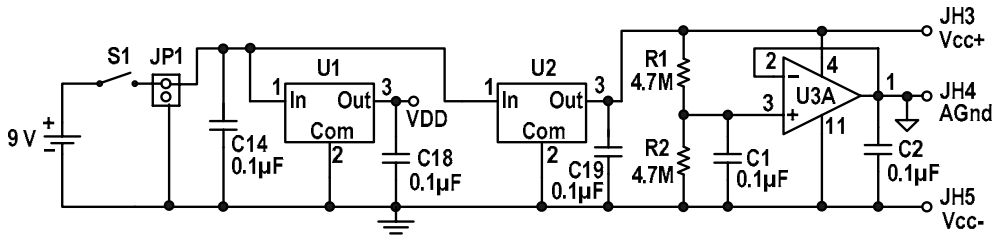

Fig. 4.5 Circuit diagram of power supply (U1, U2: LM7805, U3: LM324)

4.4.3 CM / DM ECG generator

The purpose of this circuit is to generate square wave of precise amplitude. We have two modes of operations. In CM mode, we need to have $V_{x1} = V_{x2}$ so that $V_{ed} = 0$. In the DM mode we need to have $V_{x1} = -V_{x2}$ so that $V_{ec} = 0$. A reference voltage of 1.25 V is generated using a voltage reference IC, U4. This voltage is then given to a gain control circuit built around op amp U3B as shown in Fig. 4.6. Depending on the

.

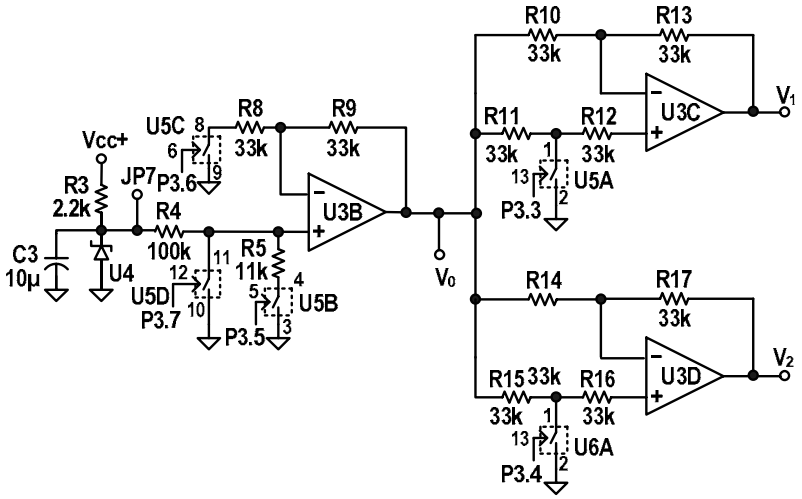

Fig. 4.6 Circuit diagram of ECG amplitude control (U5, U6: CD4066)

switch combinations, the amplitude can be scaled by 0, 0.1, 0.2 or 1.0, as given in Table 4.1. The output voltage, V_0, is given to two polarity controlled amplifiers which are controlled by switches such that the output switches between $+V_0$ and $-V_0$ for each polarity controlled amplifier.Voltage V_0 is given to two polarity controlled amplifiers (U3C, U3D). The control signals for the switches of the polarity controlled amplifier are generated by the microcontroller in such a way that V_1 and V_2 are square waves either in-phase for common mode or out-of-phase for differential mode.

Table 4.1 Switch configurations for ECG amplitude control

U5D	U5B	U5C	$V1/V_{REF}$
On	X	X	0
Off	On	Off	0.1
Off	On	On	0.2
Off	Off	Off	1.0

4.4.3 Digital controller

A 28-pin microcontroller PIC18F252 has been used for controlling the resistance variation in the impedance simulator circuit as well as for simulating CM and DM ECG signals. Main objective of using a microcontroller based circuit for control and user interface is to reduce the length of signal tracks and wires and hence possibility of external pickups. The interface is through two keys and a 16x2 LCD. Assignment of the microcontroller port pins is given in Table 4.2 and the controller circuit is shown in Fig. 4.7. Basically there are two modes of operation- ICG and ECG. In ICG, there are options for changing the frequency, *F*, basal resistance, *R*, change in resistance, *ΔR*, and the modes by which the resistance has to change, using the soft keys. The basal resistance can be selected out of four actual values of 197.83 Ω, 89.26 Ω, 60.24 Ω and 44.13 Ω. For each value of R, ΔR can be varied from 0.1 % to 0.9 % in steps of 0.1 %. The frequency of variation varied from 1 Hz to 5 Hz in steps of 1 Hz. Within ECG, there are two modes- common mode (CM) and differential mode (DM). In each of these modes, the frequency and the amplitude can be varied. The LCD shows the current mode and the value of the variable parameters.

There are two soft keys - Function and Change. The Function key selects the various options one-by-one in a cyclic manner. The parameter which is currently selected is shown blinking. The Change key allows the user to vary the parameters through a set of different choices available for it in a cyclic manner.

4.5 Software

The software has following tasks: (i) scanning the keys, (ii) updating the display, and (iii) generating ECG signal if ECG mode is selected or sending data to the digital potentiometer on SPI interface at specified intervals to generate impedance variations. The microcontroller is fed with a 20 MHz external crystal oscillator. The 20 MHz

clock is internally divided by a factor of four and the resulting clock of 5 MHz is used for the microcontroller operations. A hardware timer, timer 0 in the microcontroller is

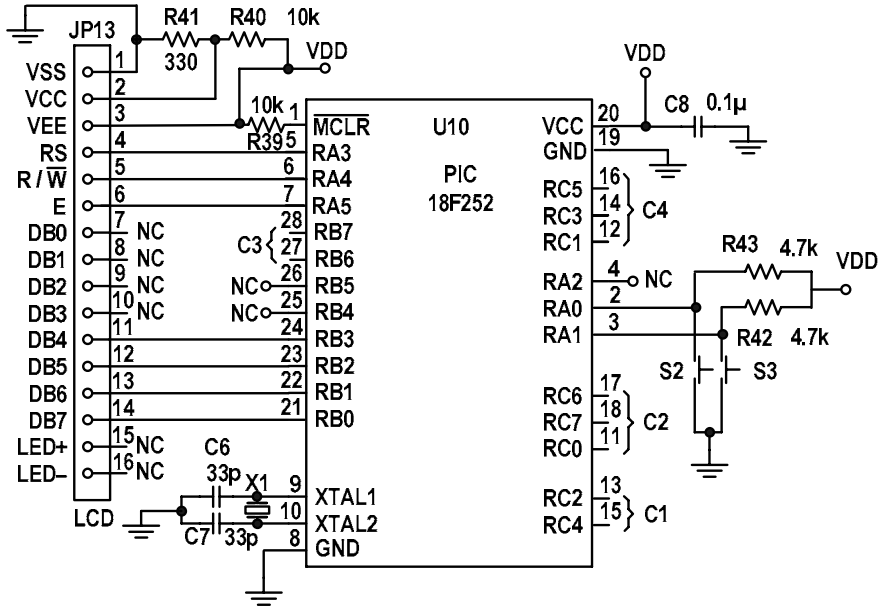

Fig. 4.7 Circuit diagram of the microcontroller circuit for user interface, resistance control, and generation of CM and DM ECG

configured in 16-bit mode to give an interrupt at every 1 ms. Since the timer registers will not get reloaded automatically, they are reloaded in the interrupt service routine. The integral multiple of this 1 ms can be used to derive other timings for ICG and ECG waveform generation, delay for key debouncing and delay necessary for writing

Table 4.2 Assignment of pins for various functions on the microcontroller

Port pin	**Function**
RB0 – RB4	LCD Data pins
RA3	Enable of LCD
RA4	RW of LCD
RA5	RS of LCD
RC6, RC7	ECG square wave generation
RC0, RC2, RC4	ECG amplitude control
RA0, RA1	Soft keys
RC1, RC3, RC5, RB6, RB7	ICG control signals

to the display. The communication with the digital potentiometer at the specified interval and ECG signal generation at the specified frequency are time critical and take very short time to perform. So these tasks are performed in the interrupt service routine of the timer 0. The other two tasks are less time critical. They are performed in the main routine. In the main routine, either of the tasks, updating the display or scanning the keys is performed in every 50 ms. For this purpose, a flag named "main loop" flag is used. This flag is set in the timer 0 interrupt service routine. The task display update has higher priority than the task "key scan". Once a key press is detected, it is confirmed in the next 20 ms. A valid key press invokes a part of the code which alters the necessary variables for the mode (ICG, ECGC or ECGD), frequency (*F*), resistance (*R*), change in resistance (ΔR) and finally marks a flag for display update. The algorithm for the main routine and the interrupt service routine are as follows.

Main Routine

Step 1: Disable all interrupts, set port pin direction registers, configure timer, enable timer interrupt and start the timer.

Step 2: Initialize the variables with default values

Step 3: Initialize the display

Step 4: If *main loop* flag is not set, go to Step 13

Step 5: Clear *main loop* flag.

Step 6: If *display update* is not marked, go to Step 8

Step7: Update display and go to step 13

Step 8: If *key confirmation* is not marked scan keys and mark for key confirmation and go to step 13

Step 9: If key de-bouncing time is not over, go to Step 12

Step 10: Clear *key confirmation* mark, scan keys and check with previous key value

Step 11: If the key press is valid, increment respective variables and mark for display update.

Step 12: Go to Step 4

Timer Interrupt Routine

Step 1: Reload timer registers

Step2: Increment the variables used for timing calculation

Step 3: If mode is not ICG, go to Step 6

Step 4: If SPI communication delay is not over, go to Step 7

Step 5: Clear SPI communication delay variable, load the value in to the SPI data register and go to Step 7

Step 6: If ECG delay is over, toggle the port pins used for ECG generation

Step 7: If main loop delay is over, set the *main loop* flag.

Step 8: Return from the interrupt routine.

4.6 Assembly and testing

The individual circuit blocks and the software have been described in the previous sections. The circuit diagram of the thorax simulator, incorporating all these blocks is shown in Fig. 4.18. The digital part of the circuit is powered by 5 V (between V_{DD} and GND) obtained using regulator IC U12 from a 9 V battery. Another 5 V regulator U13 is used to obtain supply for the analog circuits. This 5 V supply is split using U2a, giving V_{CC+}, AGND, V_{CC-}. It is to be noted that with respect to AGND, V_{CC+} = 2.5 V and V_{CC-} = -2.5 V, and with respect to GND, $V_{CC+} \approx$ 5 V, AGND ≈ 2.5 V and $V_{CC-} \approx$ 0 V. The digital control operation is handled by the microcontroller U7 (PIC18F252) with internal program memory and data RAM. Operator is controlled through two switches S1 and S2 connected to the microcontroller port pins RA0 and RA1. The LCD display is connected to the 16-pin connector J1. This is a 16 character × 2 line display with 4-bit parallel interface. Port pins RC1, RC3, RC4 are used for interfacing with the digital potentiometer U3. The analog switches U4 and U5 used for changing basal resistance are interfaced through port pins RB7 and RB6. The analog switches U9B, U9C, and U9D used for ECG amplitude control are connected to the microcontroller through port pins RC0, RC2, and RC4. The port pins RC6 and RC7 connected to U8A and U8B are used to control ECG mode.

For the circuit diagram in Fig. 4.18, PCB layout, for a 12 mm × 12.5 mm double sided PCB with plated through hole (PTH), was prepared with a large ground plane on the component side. After fabrication of the PCB, all the components were assembled on the PCB. The track layout of the component and solder sides and the component placement on the PCB are given in Appendix C. We refer to this assembled instrument as THS-06.

For testing the resistance variation of the circuit, it was excited, across terminals I1 and I2 with a 100 kHz 5 V_{p-p} sinusoidal waveform from a function generator (Agilent 333120A) in series with a fixed resistance of 560 Ω and the

voltage developed across the terminals E1 and E2 was measured with an oscilloscope (Tektronix TDS5054). The observed voltage was used for calculating the resistance across the terminals. The calculated and observed values of sinusoidal resistance variation are given in Table 4.3.

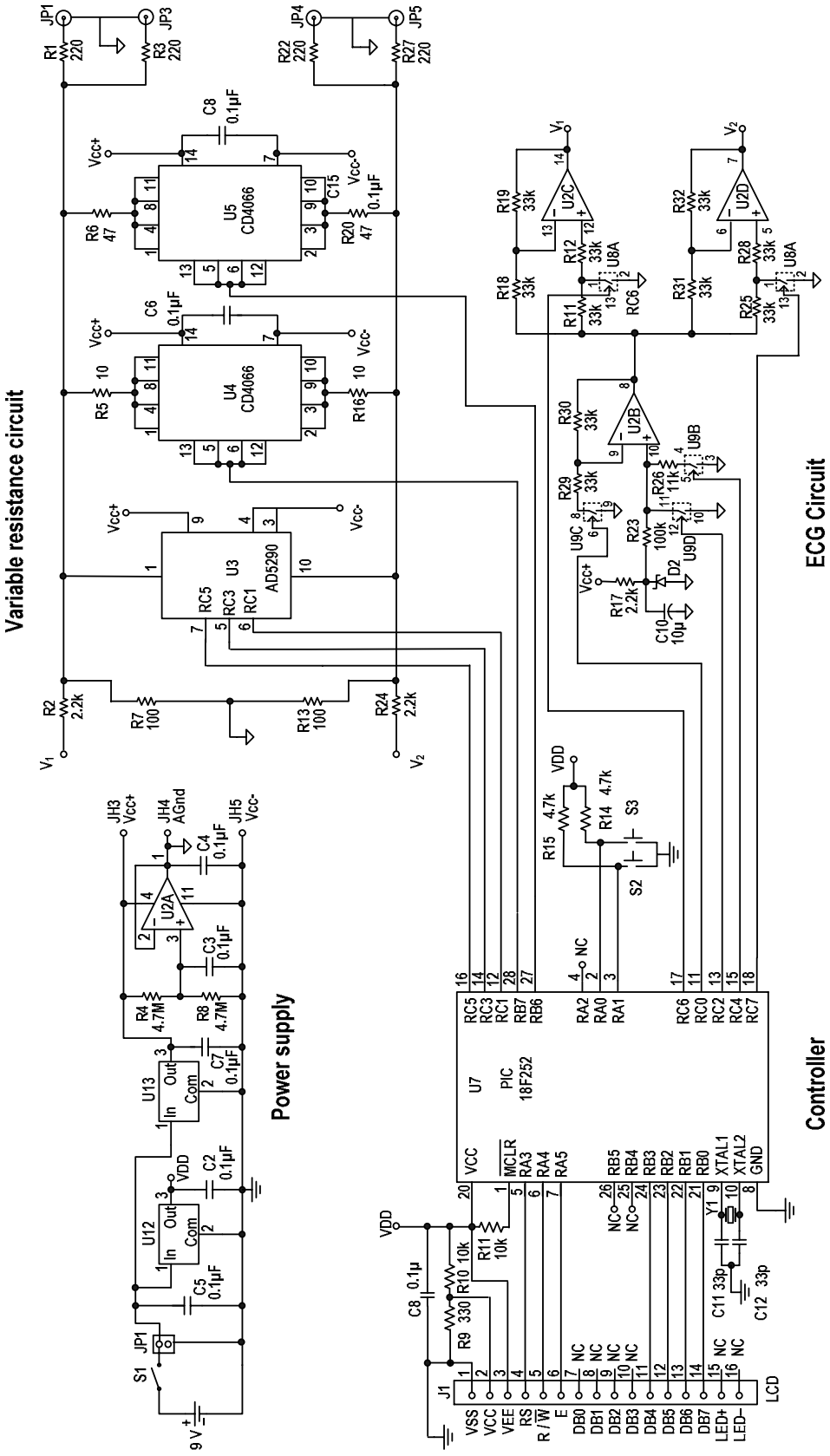

Fig. 4.8 Complete circuit diagram of thorax simulator

Table 4.3 Basal resistance R for different switch status and resistance variation ΔR for digital potentiometer setting

Switch status		**Calculated**			**Measured**		
S1	**S2**	**R(Ω)**	**ΔR(Ω)**	**ΔR/R(%)**	**R(Ω)**	**ΔR(Ω)**	**ΔR/R(%)**
0	0	197.83	0.00	0.0	197.83	0.00	0.00
			0.20	0.1	197.44	0.36	0.18
			0.40	0.2	197.15	0.65	0.33
			0.59	0.3	196.94	0.86	0.43
			0.79	0.4	196.66	1.14	0.57
			1.00	0.5	196.36	1.44	0.73
			1.19	0.6	196.13	1.67	0.85
			1.39	0.7	195.84	1.96	0.99
			1.58	0.8	195.57	2.23	1.13
			1.78	0.9	195.17	2.63	1.33
0	1	89.26	0.00	0.0	89.26	0.00	0.00
			0.09	0.1	89.07	0.13	0.15
			0.18	0.2	88.88	0.32	0.36
			0.27	0.3	88.76	0.44	0.49
			0.36	0.4	88.67	0.54	0.60
			0.45	0.5	88.58	0.62	0.70
			0.54	0.6	88.40	0.80	0.90
			0.62	0.7	88.30	0.90	1.01
			0.71	0.8	88.13	1.07	1.20
			0.80	0.9	88.00	1.20	1.35
1	0	60.24	0.00	0.0	60.24	0.00	0.00
			0.06	0.1	60.10	0.10	0.17
			0.12	0.2	59.96	0.24	0.4
			0.18	0.3	59.86	0.34	0.56
			0.24	0.4	59.75	0.45	0.75
			0.30	0.5	59.66	0.54	0.90
			0.36	0.6	59.51	0.69	1.15
			0.42	0.7	59.34	0.86	1.43
			0.48	0.8	59.26	0.95	1.57
			0.54	0.9	59.15	1.05	1.75
1	1	44.13	0.00	0.0	44.13	0.00	0.00
			0.04	0.1	44.04	0.06	0.13
			0.09	0.2	43.95	0.15	0.35
			0.13	0.3	43.90	0.20	0.45
			0.18	0.4	43.87	0.23	0.52
			0.22	0.5	43.76	0.35	0.78
			0.27	0.6	43.70	0.40	0.90
			0.31	0.7	43.63	0.47	1.06
			0.35	0.8	43.59	0.51	1.15
			0.40	0.9	43.54	0.56	1.28

Chapter 5
ICG HARDWARE DEVELOPEMENT

5.1 Introduction

As mentioned in Section 3.4, hardware sections of the prototype of the ICG instrument developed in the lab [14][15][16], are: signal source, demodulator, and drift cancellation circuit. For this purpose, the performance of existing circuits was analyzed, alternatives evaluated, and a modified or new version of the circuit was finalized. All the blocks were integrated on one PCB, with layout specially designed for reducing noise and pick-up. This chapter presents this hardware development.

5.2 Signal source

As mentioned in Section 2.4, the mean impedance of the thorax is about 20 Ω and change in impedance is 0.1 to 0.2 Ω [5][6]. The variation in the impedance is 0.5 % to 1 % of the basal impedance. The spectral content of ICG signal is in the range of 0 to 15 Hz [17]. Since the ICG signal is extracted from the amplitude modulated voltage signal sensed through the sensing electrodes, the injected carrier current amplitude should be stable enough to meet the above criteria. It was decided to study the performance of the Wein bridge oscillator circuit in the existing prototype, and work out alternatives.

5.2.1 Evaluation of oscillators developed earlier at IIT Bombay for ICG instrument

The Wein bridge oscillator circuit used by Manigandan [15] as the voltage source for the V/I converter driving the current electrodes is shown in Fig. 5.1. It was modified by Naidu [16], as shown in Fig. 5.2, to increase its short term stability [24][25]. A quadrature oscillator was also developed by Naidu [16] which is shown in Fig. 5.3. The amplitude of the oscillator output is measured with a digital storage oscilloscope (Agilent 54621D) at different time base setting from 1 μs/division to 500 ms/division

with amplitude resolution set at 20 mV/division, to measure the amplitude range of variations in different frequency regions. The short term amplitude variations measured as variations in the positive peak output of the oscillator circuits of Fig. 5.1, 5.2, and 5.3 were found to be 60 – 130 mV, 50 - 110 mV, and 45 - 100 mV. The above measurements were done in the positive peak of 5 V peak-to-peak outputs. The short term amplitude instability in the three oscillator circuits are 2.4 - 5.2 %, 2.0 - 4.4 %, and 1.8 - 4.0 % of the positive peak respectively.

5.2.2 Modified Wien bridge oscillator

The Wien bridge oscillator was modified with a new amplitude stabilization loop for better short term amplitude stability [24]. The circuit diagram of modified Wien bridge oscillator is shown in Fig. 5.4. The amplitude stabilization loop consists of a peak detector and an error amplifier. The output of the oscillator was given through the diode D1 to the error amplifier. The error amplifier has two inputs. The output of

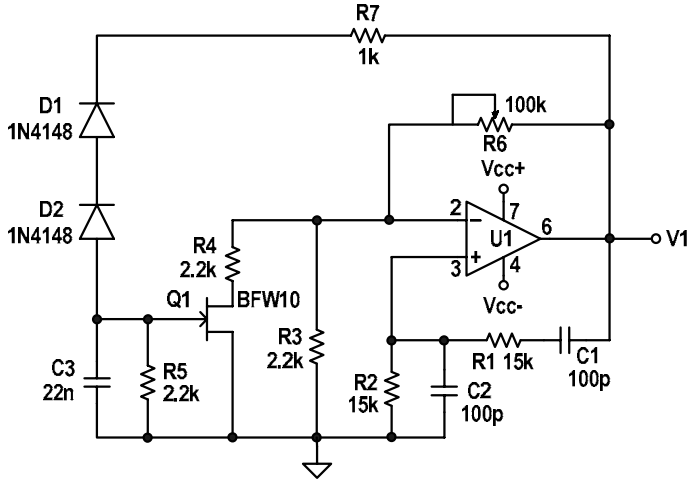

Fig. 5.1 Wein bridge oscillator used by Manigandan [15] (U1: LF356)

peak detector was given to the inverting input of the error amplifier and the non-inverting input of the error amplifier was fed with a reference voltage. The amplitude of the oscillator output can be varied by changing this reference voltage. The reference voltage can be between 0 to $(V_o)_{max}$. The output from the error amplifier is connected to the gate of the JFET, which was configured as a voltage controlled resistor. The output from the error amplifier is a low pass filtered comparator output. The error amplifier compares the reference voltage and the peak detector output. Whenever the peak detector output becomes more positive than the set point, the

comparator output goes to negative saturation. This negative voltage was given to the gate of the JFET, which reduces the gain of the oscillator by increasing the input resistance of the oscillator.

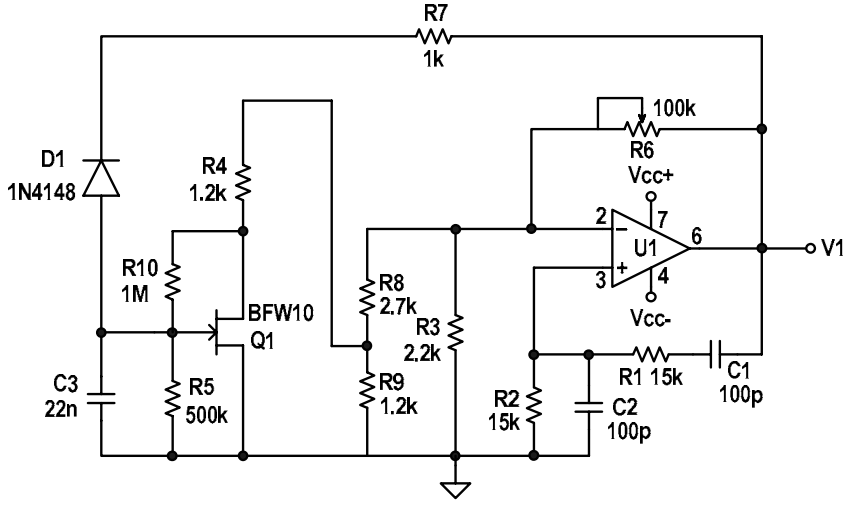

Fig. 5.2 Wein bridge oscillator used by Naidu [16] (U1: LF356)

5.2.3 High-frequency precision function generator

It was decided to test an IC MAX038 based oscillators. MAX038 is a high-frequency precision function generator with selectable output of sine, square, saw tooth or triangle and pulse waveforms. The circuit diagram of the oscillator using IC MAX038 is given in Fig. 5.5. The frequency of oscillation is decided by the input resistor R_{in} and the capacitor C_F. For any frequency between 0.1 Hz to 20 MHz, the value of R_{in} and C_F can be obtained from

$$F_O = \frac{5}{R_{in} C_F} \qquad (5.1)$$

For 100 kHz sine wave, we selected R_{in} = 15.5 kΩ and C_F =330 pF. The A_0 and A_1 pins of MAX038 were connected to ground and V_{cc+} respectively to select the internal multiplexer to output sine wave. This work was jointly done with J. N. Sarvaiya [26] who worked on developing an impedance glottograph.

5.2.4 Comparisons of short-term amplitude stability of different oscillators

The amplitude variations were measured at different time setting from 1 μs/division to 500 ms/division on different oscillators discussed above. For the comparison purpose, the output amplitude of the oscillators was set at 5 V peak-to-peak. The short term

amplitude instability in the Wien bridge oscillator in the existing instrument (Fig. 5.1), Wien bridge oscillator developed by Naidu [16] (Fig. 5.2), and the quadrature phase shift oscillator developed by Naidu [16] (Fig. 5.3) varied about 2. - 5.2 %, 2.0 - 4.4 %, and 1.8 - 4.0 % respectively of the positive peak of the output. For the three oscillators discussed above, the amplitude variations increased when measured with the time base setting form 1 μs/ division to 20 ms/ division and the

.

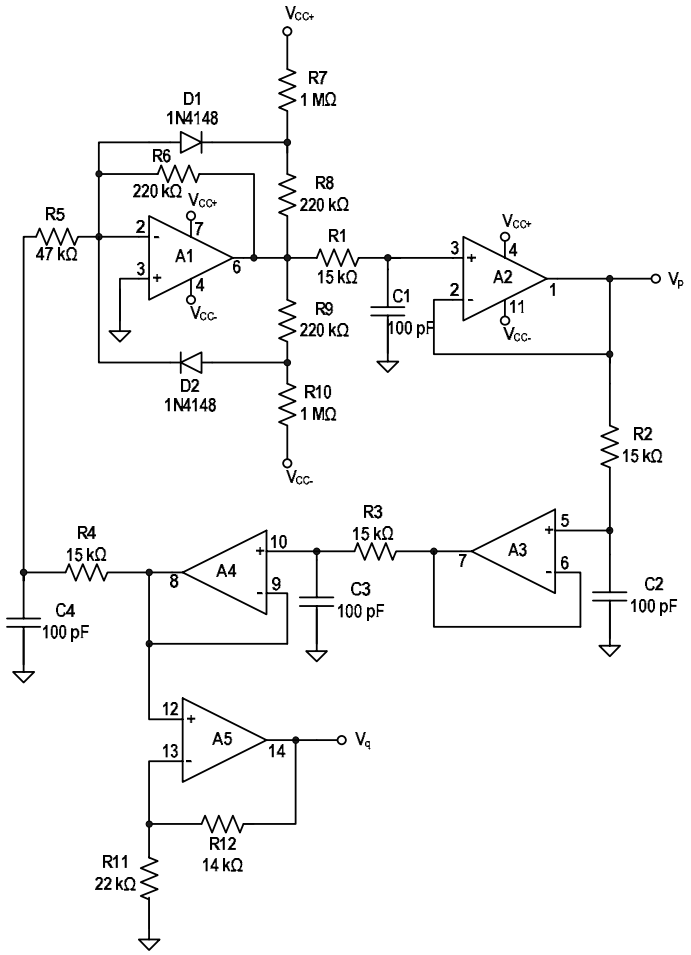

Fig. 5.3 Phase shift oscillator used by Naidu [16]

(A1 – A5: LF356)

amplitude variations remaind the same for the time base setting above 20 ms/division. For the modified Wien bridge oscillator of Fig. 5.4, the amplitude variations were 0.08 - 0.67 % of the positive peak of the output. For the modified Wien bridge oscillator, the amplitude variations decreased when measured with the time base setting was increased from 1 μs/ division to 1 ms/ division, remained the same for the time base setting above 1 ms/division.

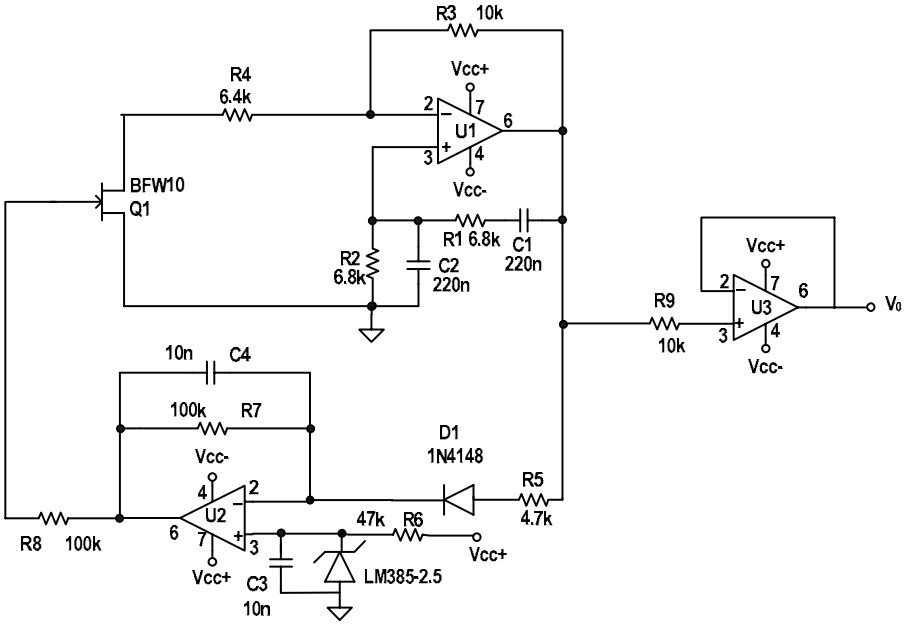

Fig. 5.4 Modified Wien bridge oscillator (U1 – U3: LF357)

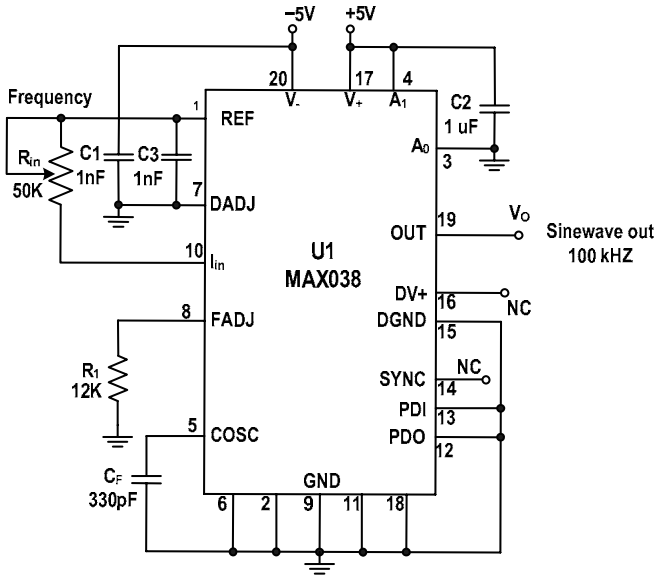

Fig. 5.5 High-frequency precision function generator

The amplitude variations were similarly measured for the sinusoidal source circuits of modified Wien bridge oscillator of Fig. 5.4 and MAX038 based function generator of Fig. 5.5. Since the output of the high-frequency precision function generator is 2 V peak to peak, the output amplitude of modified Wien bridge oscillator was set at 2 V (p-p) by setting the reference voltage at 2 V for comparison

purpose. The amplitude variations in the modified Wien bridge oscillator were 0.22 - 0.97 % of the positive peak of the output. For the high-frequency precision function generator, the amplitude variations were 0.97 - 1.50 %. These amplitude variations decreased as the time-base setting of the oscilloscope was increased from 1 μs/division to 200 μs/division and they increased as the time-base increased form 200 μs/division to 2 ms/division. The amplitude variations remained the same for the time base settings from 2 ms/division to 20 ms/division and then decreased for 20 ms/division to 500 ms/division. The modified Wien bridge oscillator of Fig. 5.4 exhibited better short term amplitude stability than the other oscillator circuits tested. Hence it was decided to use the modified Wien bridge oscillator of Fig. 5.4 as signal source.

5.3 Voltage-to-current converter

The circuit diagram of the voltage-to-current converter in the existing instrument is shown in Fig 5.6. The excitation current is given as

$$I = \frac{V_1}{R_7} \tag{5.2}$$

The V/I converter also has a 2.2 kΩ resistance in parallel with the excitation electrode path. This limits the dc voltage gain of the circuit and prevents the opamp from going into saturation in case of loose skin-electrode contact. The current from the V/I converter is fed to the outer current injecting electrode pair I1 and I2 of the four-electrode configuration through DC blocking capacitors. In this current source,

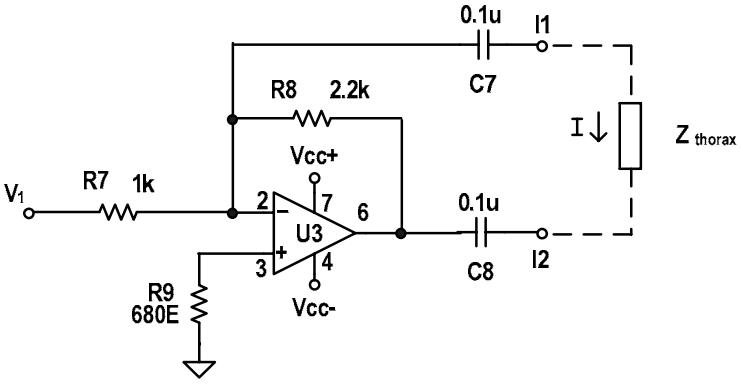

Fig. 5.6 Excitation circuit used in the existing instrument [15]

(U3: LF356)

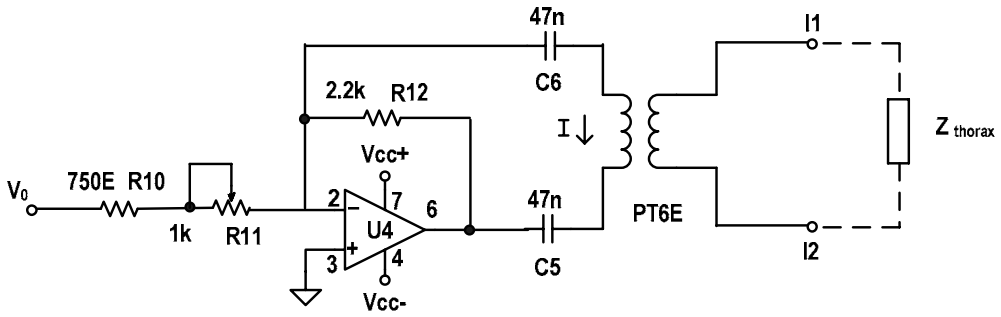

Fig. 5.7 High frequency transformer-based balanced excitation circuit (U3: LF357)

one of the nodes is at virtual ground. Hence the two terminal voltages are unbalanced with respect to ground. This leads to the possibility of stray currents and common mode pick-ups. A high frequency transformer-based balanced excitation circuit is used to solve this problem as shown in Fig. 5.7. In the new circuit the excitation current is given as

$$I = \frac{V_0}{R_{10} + R_{11}} \tag{5.3}$$

There is bound to be coupling loss due to transformer, but it provides isolation and helps in pick-up rejection

5.4 ICG extraction circuit

The ICG extraction circuit has two major sections: the instrumentation amplifier section and the demodulator and filter section.

5.4.1 Instrumentation amplifier

The instrumentation amplifier used in the existing instrument is a conventional 3 opamp configuration as shown in Fig. 5.8. This is configured to give a differential gain around 10. This circuit was evaluated for CMRR and phase delay at the operational frequency of 100 kHz. An instrumentation amplifier based on single chip instrumentation amplifier INA128 which is shown in the Fig. 5.9 also was evaluated for 'CMRR' and phase delay at the operational frequency of 100 kHz. The differential gain of the single chip instrumentation amplifier was kept at 10 for the comparison.

purpose. The differential gain A_d of the single chip instrumentation amplifier is given as

$$A_d = 1 + \frac{50000}{R_{16} + R_{17}} \tag{5.4}$$

It was observed that the CMRR of the conventional instrumentation amplifier used in the existing circuit is 45.3 dB and the phase lag between input and output is 23° and same for the single chip instrumentation amplifier is 47.8 dB and 6° respectively. Hence it was decided to use the single chip instrumentation amplifier.

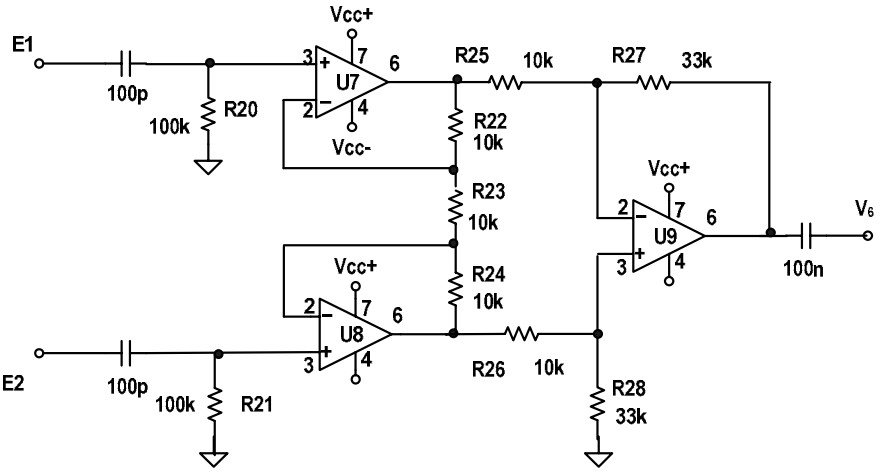

Fig. 5.8 Instrumentation amplifier used in the existing instrument [15]

(U7 – U9: LF356)

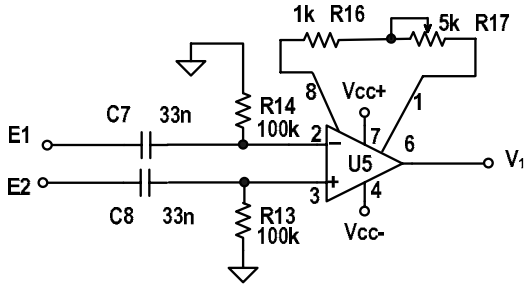

Fig. 5.9 Single chip instrumentation amplifier (U5: INA128)

5.4.2 Demodulator section

The demodulator section in the existing instrument is shown in Fig. 5.10. It consists of a conventional precision rectifier and a low pass filter to get the envelope of the amplitude modulated waveform. But at 100 kHz, because of phase shifts and switching delay, the amplitudes of the positive and negative half cycles do not properly align, this result in distorted rectified output. Another configuration of precision rectifier is shown in Fig. 5.11 [27]. In this configuration, the opamp used for

rectification is active for both the half cycles of the input signal and gives better output as compared to the previous one. The input and output waveforms of both the circuits are given in Fig. 5.12 and Fig. 5.13. As the modified circuit gives satisfactory full-wave rectification at excitation frequency (100 kHz), it has been selected for use in the new design.

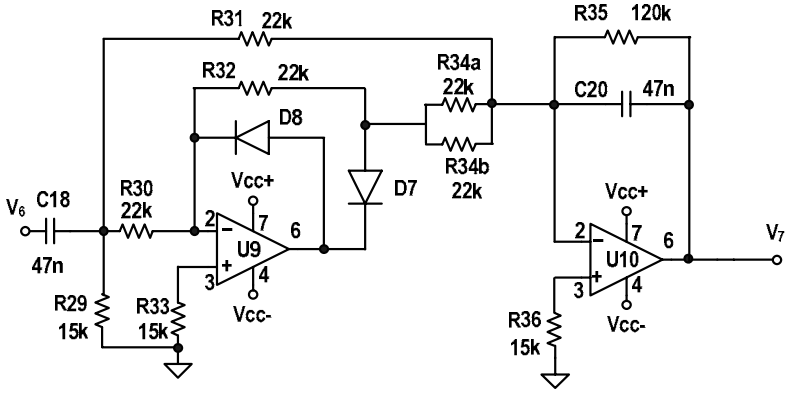

Fig. 5.10 Demodulator circuit in the existing instrument [15] (U9, U10: LF356)

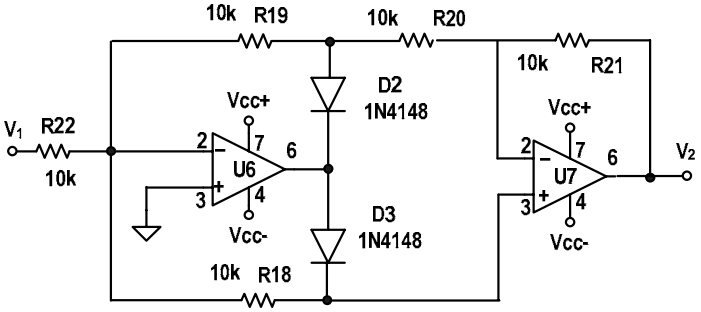

Fig. 5.11 Modified precision rectifier [27] (U6, U7: LF357)

5.5 Contact impedance indicator

The contact impedance indicator circuit was designed to ensure proper contact of the electrode with the skin. The output of the precision rectifier is buffered and given to the non inverting input of a comparator. The inverting input of the comparator is fed with voltage corresponding to the nominal thoracic impedance through a simple voltage divider network. When the electrode contact is not proper with the skin, the precision rectifier output will be more than the voltage corresponding to the nominal

thoracic impedance. This switches the comparator output to the positive saturation and turn on the LED connected to the output.

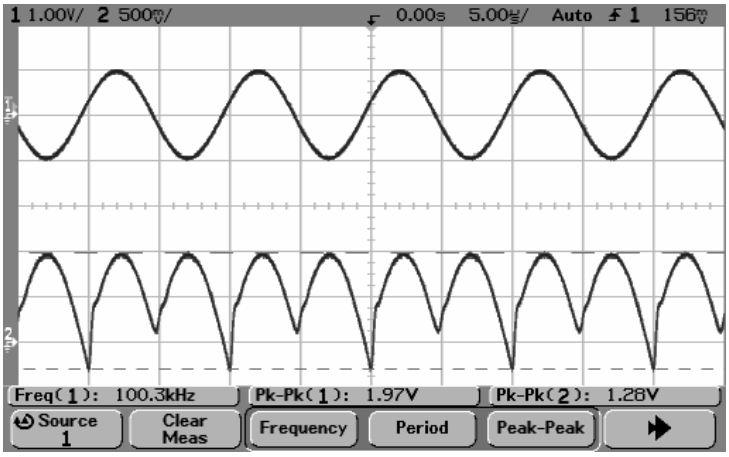

Fig. 5.12 Input and output waveforms of precision rectifier circuit of Fig. 5.10 (when C20 removed)

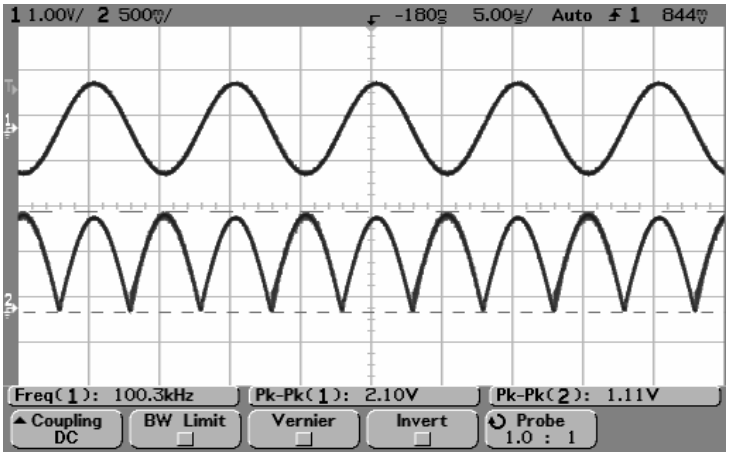

Fig. 5.13 Input and output waveforms of modified precision rectifier of Fig. 5.11

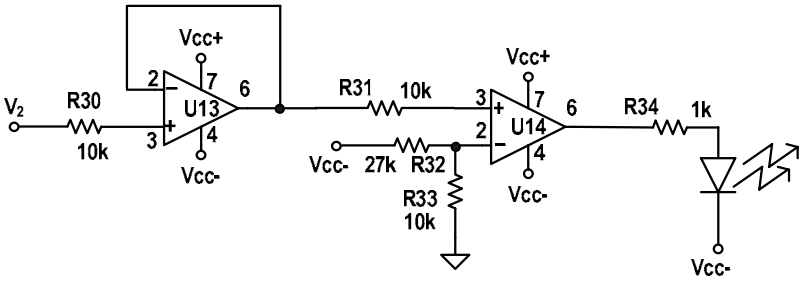

Fig. 5.14 Circuit diagram of contact impedance indicator (U13, U14: LF357)

5.6 Base-line restoration circuit

In the sensed thoracic impedance signal, the amplitude of the varying thoracic impedance signal is typically 1 to 2% of the basal impedance [5][6]. This varying impedance is contaminated by respiratory and motion artifacts. These artifacts result in large base-line drift as compared to the varying impedance signal. Thus if the signal is used as such, only a portion of the available input dynamic range of ADC will be used for analysis of the signal. Therefore, it is important to partly remove the base-line drift for the effective use of input dynamic range of ADC.

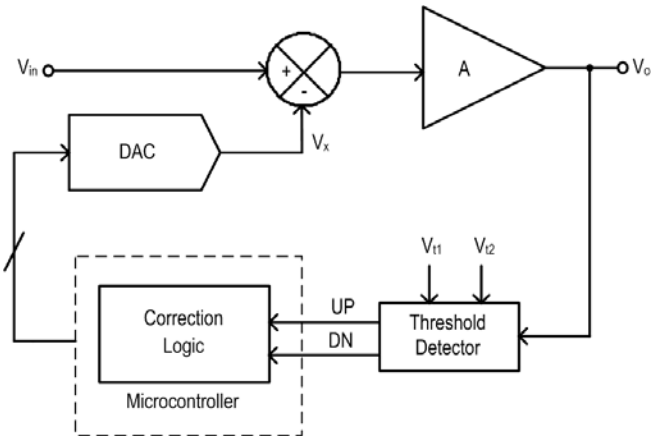

Fig. 5.15 Block diagram of drift cancellation circuit

As a solution to this problem, a microcontroller based drift cancellation circuit was developed. Block diagram of the technique is shown in Fig. 5.15 and the detailed description is given in Appendix A. In this circuit, whenever the output voltage crosses the range set by two pre-defined thresholds, it is detected by comparison and the correction voltage is estimated and subtracted or added to the signal to bring the output within the middle of threshold range. It was decided to use this circuit for drift cancellation from z(t) waveform. The circuit schmatic is given in Fig. 5.16. Threshold

voltages, V_{t1} and V_{t2}, are obtained by using a resistive voltage divider. The output voltage is compared with the thresholds using comparators, U1B and U1C, and the outputs of the comparators are connected to port pins P1.0 and P1.1 of the microcontroller. The tracking up/down counter is realized using software inside the microcontroller. The count value is output to a DAC as an approximation to the baseline drift. This work was jointly done along with Mr. Vinod Kumar Pandey.

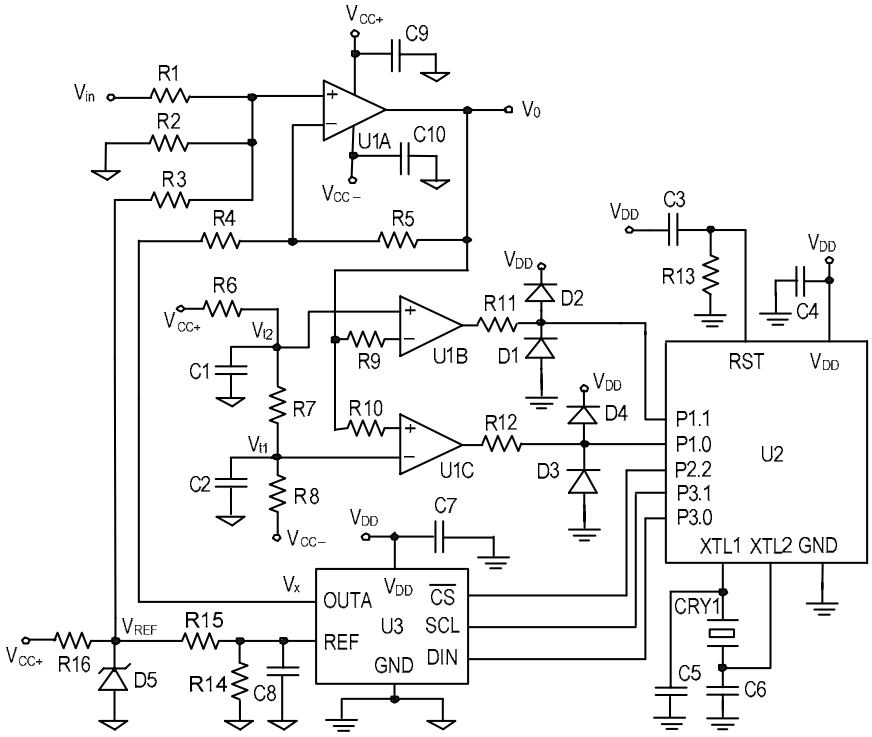

Fig. 5.16 Circuit diagram of the microcontroller based implementation

5.7 ECG amplifier

The ECG amplifier is a part of the impedance cardiograph and is used to acquire the ECG simultaneously with the ICG signal. This ECG signal is used as a fiducial mark for ensemble averaging of the ICG signal to calculate the cardiac output. The ECG amplifier is connected to the voltage pickup electrodes E1 and E2 of the ICG extraction circuit. The filter section in the instrumentation amplifier section eliminates the ICG signal from being picked up by this amplifier. The circuit diagram of the ECG amplifier to be used in the new design is shown in the Fig. 5.17. The filter

section of the circuit was adapted from Manigandan [15] and the instrumentation amplifier section of the circuit used by Manigandan [15] was replaced with a single chip instrumentation amplifier. The low pass filter cut-off was kept at 22 Hz and the high pass filter cut-off was kept at 1.6 Hz. The portion of signal which is of interest to ICG is the QRS complex, which falls well with in this pass band.

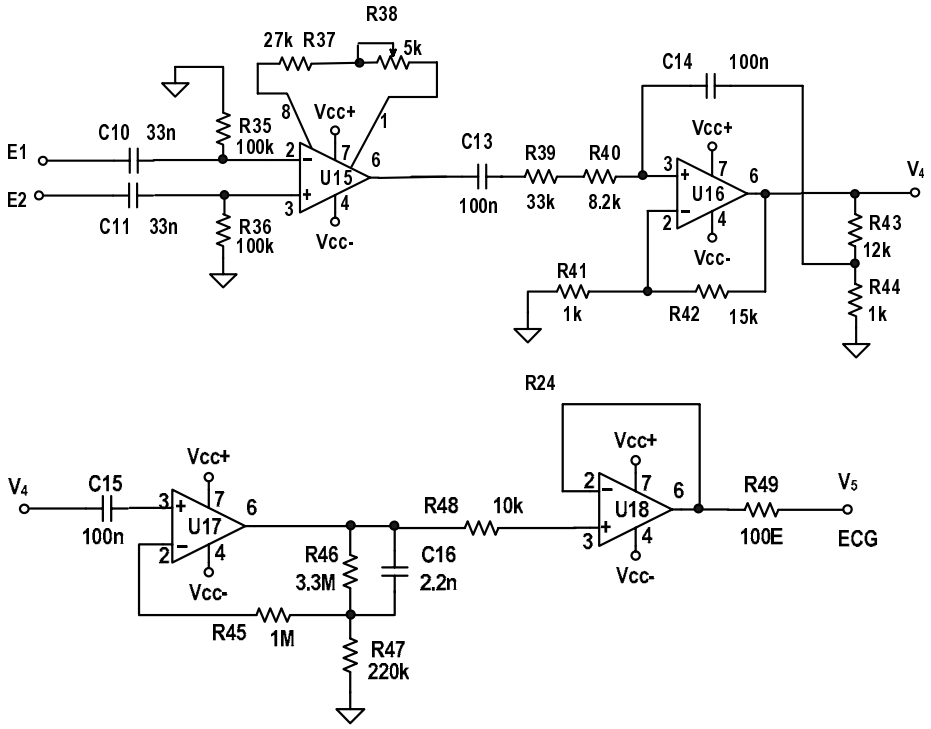

Fig. 5.17 Circuit diagram of the ECG amplifier [15] (U15 – U18: LF357)

5.8 Overall circuit assembly and testing

In the pervious sections, various circuit options for each block have been discussed. Based on the detailed testing, the overall hardware was assembled, with the circuit diagram as shown in Fig. 5.18. It consists of

a) Modified Wien bridge oscillator (Fig. 5.4), with IC U1 and U4,
b) High frequency transformer-based balanced excitation circuit (Fig. 5.7), with IC U2,
c) Voltage sensing amplifier using single chip instrimentation amplifier (Fig. 5.9), with IC U5,
d) Modified precision rectifier (Fig. 5.11), with IC U6 and U7,
e) Contact impedance indicator (Fig. 5.14), with IC U11,

f) Base-line restoration circuit (Fig. 5.16), with IC U22, U23, U24, U25, and U26,ECG amplifier (Fig. 5.17), with IC U17, U18, U19, and U20.

The circuit is powered by a ±9 V source, which is regulated to V_{CC+} (+5 V) and V_{CC-}(-5 V) using linear regulators U9 (7805) and U15 (7905). The base-line restoration circuit is powered by separate 9 V supply and 5 V regulator U27 (7805), in order to limit any contamination of the analog supply by digital noise. The base-line restoration part of the circuit is separately shown in Fig. 5.19.

For the circuit diagram in Fig. 5.18 and 5.19, PCB layout, for a 16 mm × 15 mm double sided PCB with plated through hole (PTH), was prepared with a large ground plane on the component side. After fabrication of the PCB, all the components were assembled on the PCB. The track layout of component and, solder sides, and the components placement on the PCB are given in Appendix C. We refer to this assembled instrument as ICG-06.

5.8.1 Testing of the hardware with thorax simulator

The output of the ICG instrument ICG-06 was tested by connecting it to the thorax simulator THS-06 with basal resistance set at 44.13 Ω and change in resistance set at 0.1%. The waveforms for sinusoidal change and step change at 1 Hz and 5 Hz are shown in Fig. 5.20 and Fig. 5.21 respectively.

5.8.2 Acquiring ICG from subjects

We made recordings using our instrument ICG-06 and a widely used instrument HIC 2000 [28] from Bio-Impedance Technology (Connecticut, U.S.A.) using spot electrodes as well as band electrodes, in order to have appropriate comparison. The recordings were taken on a healthy subject under normal conditions with band as well as spot electrodes. The ICG signal recorded simultaneously along with the ECG signals from subject LV with band and spot electrodes are shown in Fig. 5.22 and Fig. 5.24 respectively. These signals were directly acquired from the impedance cardiograph ICG-06 using a data acquisition unit (Keithley KUSB 3102) with sampling rate of 1 k Sa/s. These signals were then digitally filtered using filters developed in SPI Lab by Vinod. K. Pandey to remove the noise and motion artifacts. The filtered waveforms are shown in Fig. 5.23 and Fig. 5.25. Recordings were done on the same subject with the instrument HIC 2000 using band and spot electrodes.

The acquired waveforms using band and electrodes are shown in Fig. 5.26 and Fig. 5.28, and the filtered waveforms are shown in Fig. 5.27 and Fig. 5.29.

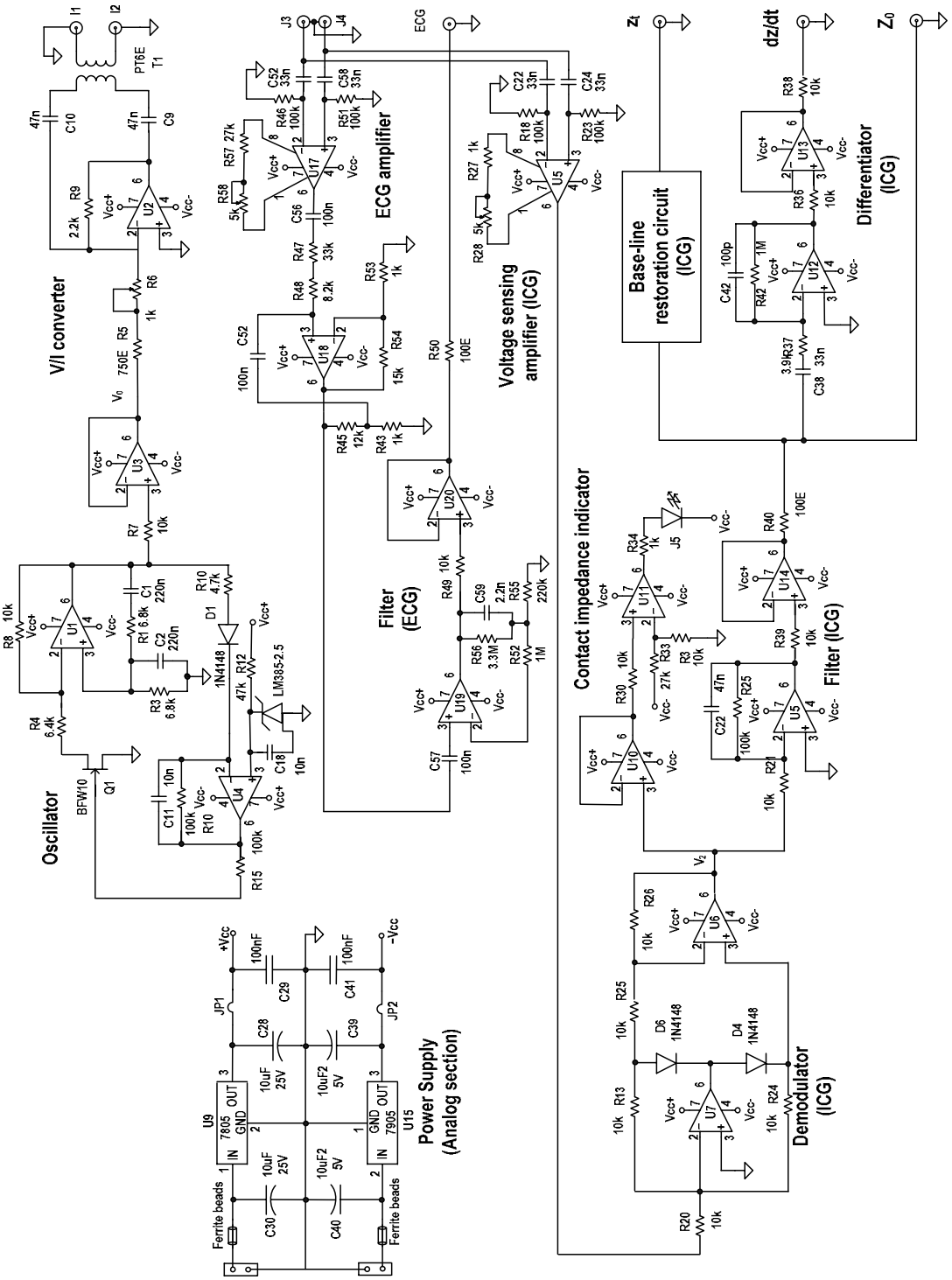

Fig. 5.18 Complete circuit diagram of ICG hardware

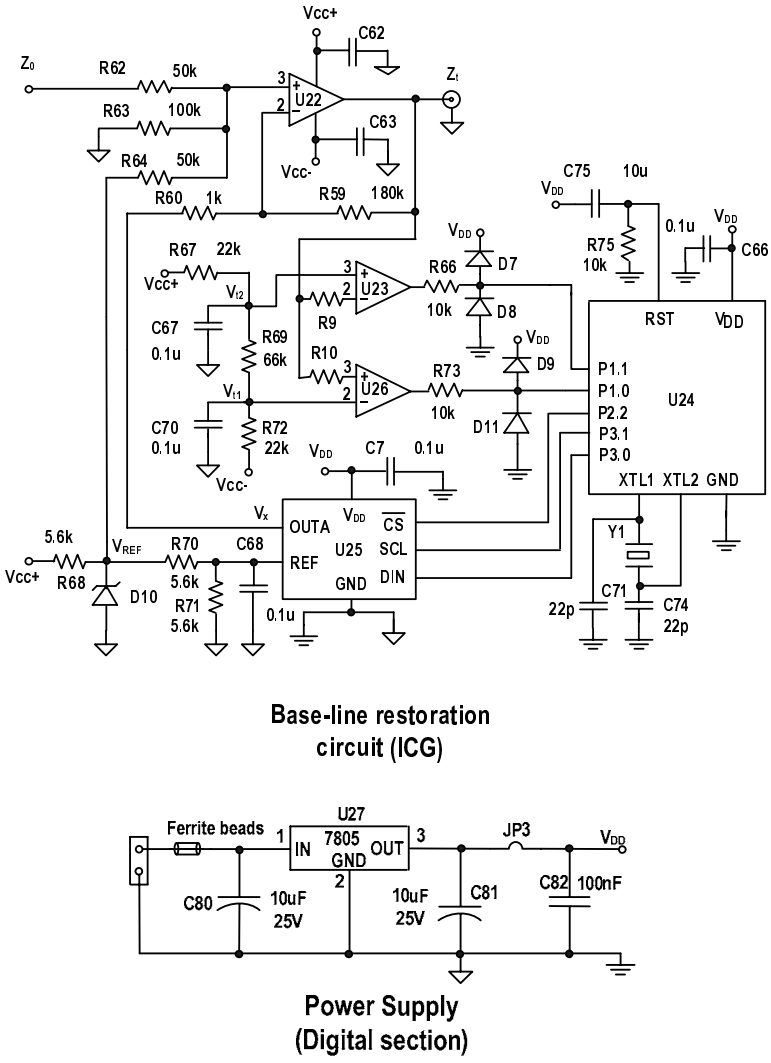

Fig. 5.19 Base-line restoration circuit.

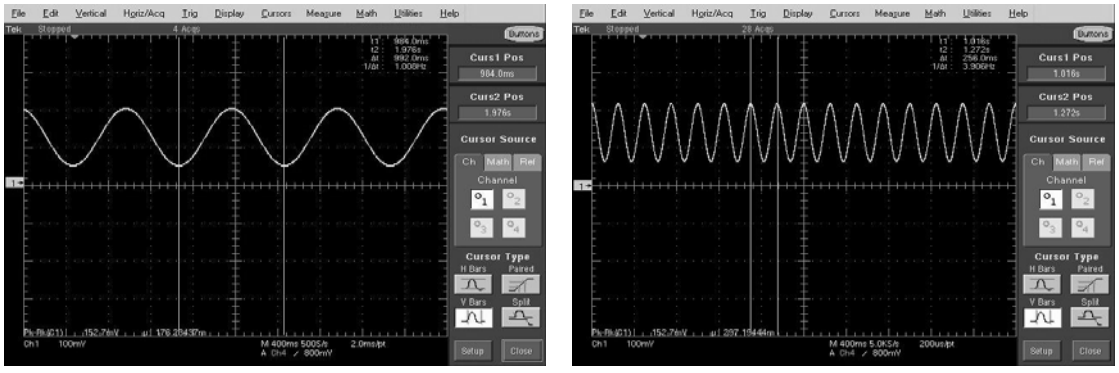

(a) (b)

Fig. 5.20 Output waveform z(t) from ICG-06 connected to thorax simulator THS-06, for sinusoidal change in resistance with frequency of (a) 1 Hz (b) 5 Hz. R = 44.1 Ω, $\Delta R/R = 0.001$

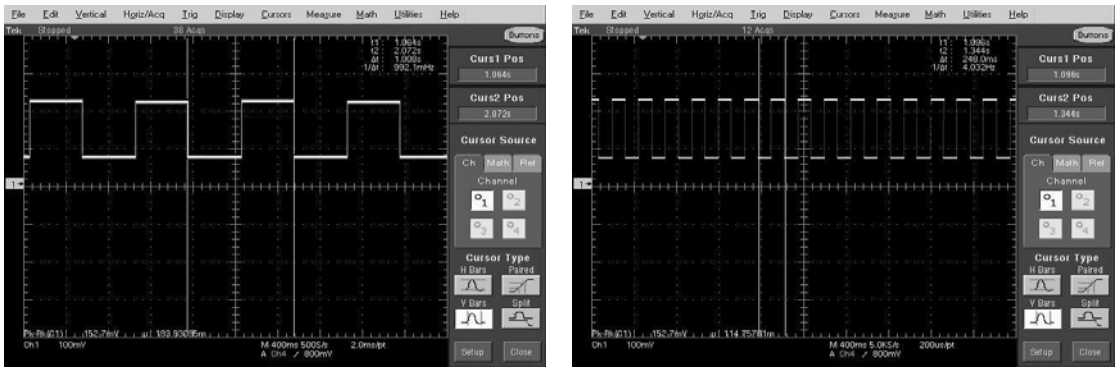

(a) (b)

Fig. 5.21 Output waveform z(t) from ICG-06 connected to thorax simulator THS-06, for step change in resistance with frequency of (a) 1 Hz (b) 5 Hz. R = 44.1 Ω, $\Delta R/R = 0.001$

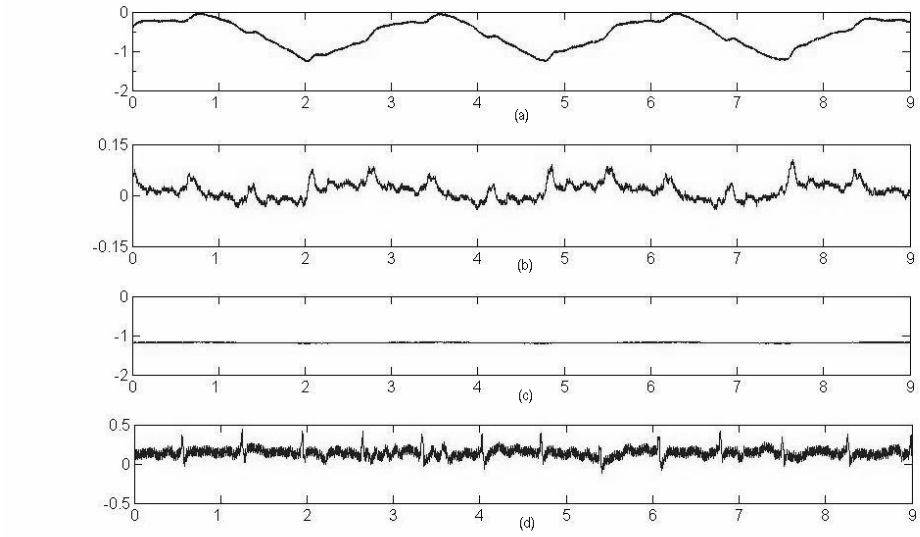

Fig. 5.22 Signals recorded from subject LV with ICG-06 instrument using band electrodes (a) $-z(t)$, (b) $-dz/dt$, (c) $-Z_0$, and (d) ECG (x axis: seconds, y axis: arbitrary unit).

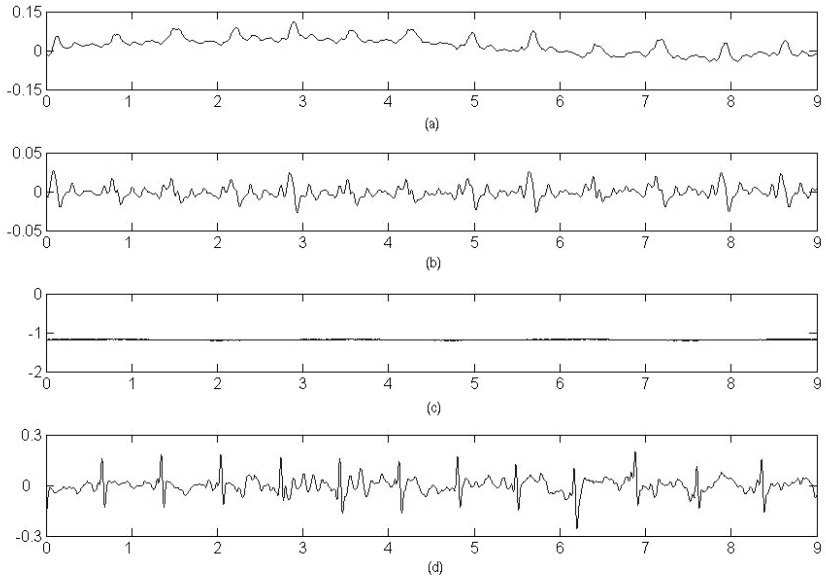

Fig. 5.23 Processed output of signal in Fig. 5.22 (a) *-z(t)*, (b) *-dz/dt*, (c) $-Z_0$, and (d) ECG (x axis: seconds, y axis: arbitrary unit).

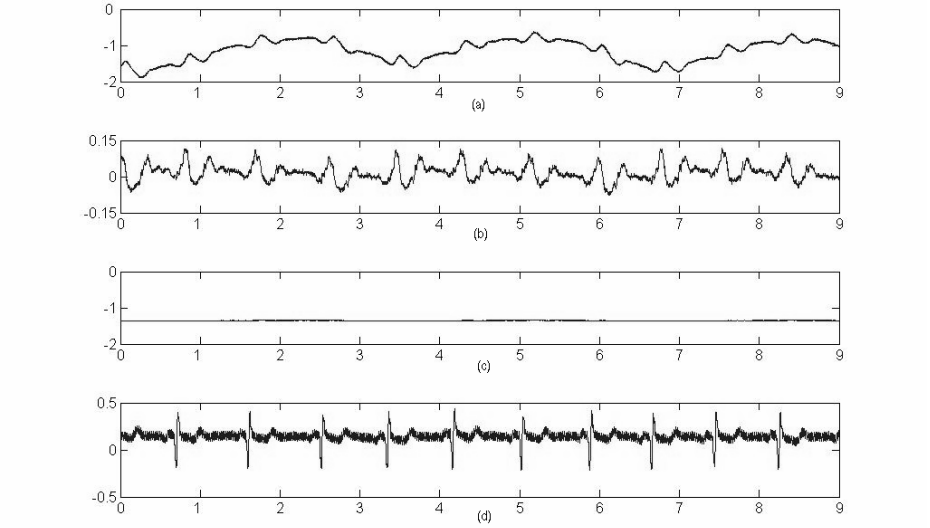

Fig. 5.24 Signals recorded from subject LV with ICG-06 instrument using spot electrodes. (a) *-z(t)*, (b) *-dz/dt*, (c) $-Z_0$, and (d) ECG (x axis: seconds, y axis: arbitrary unit).

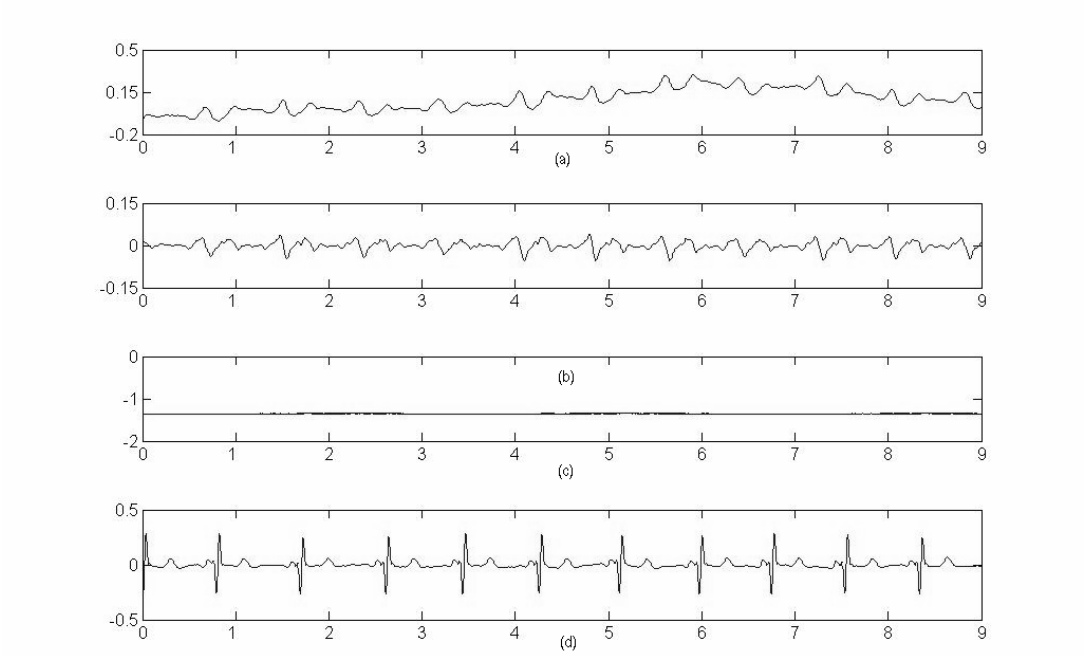

Fig. 5.25 Processed output of signal in Fig. 5.24 (a) *-z(t)*, (b) *-dz/dt*, (c) $-Z_0$, and (d) ECG (x axis: seconds, y axis: arbitrary unit).

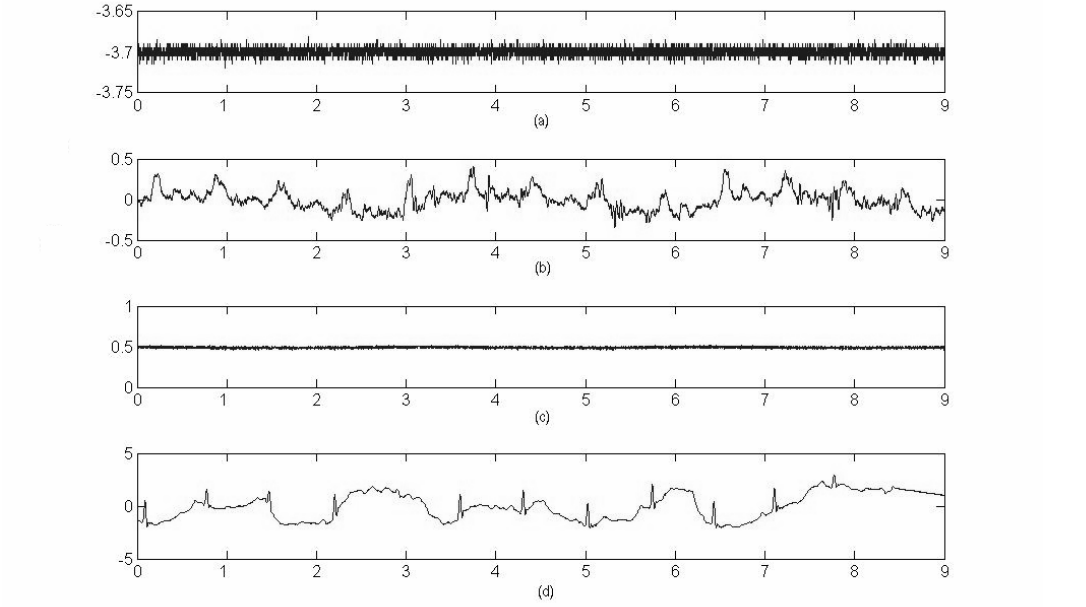

Fig. 5.26 Signals recorded from subject LV with HIC 2000 instrument using band electrodes (a) *z(t)*, (b) *-dz/dt*, (c) Z_0, and (d) ECG (x axis: seconds, y axis: arbitrary unit).

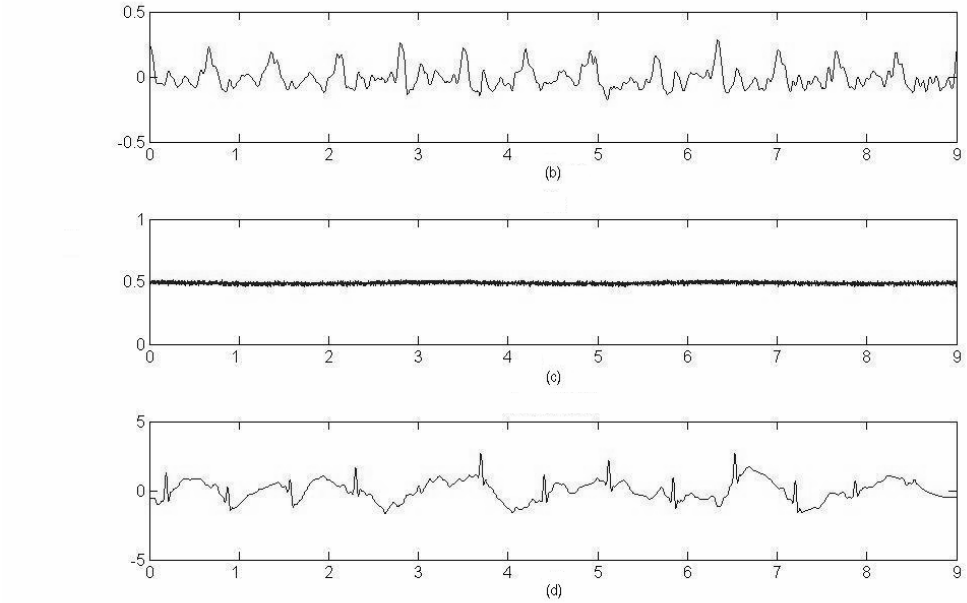

Fig. 5.27 Processed output of signal in Fig. 5.26 (b) *-dz/dt*, (c) Z_0, and (d) ECG (x axis: seconds, y axis: arbitrary unit).

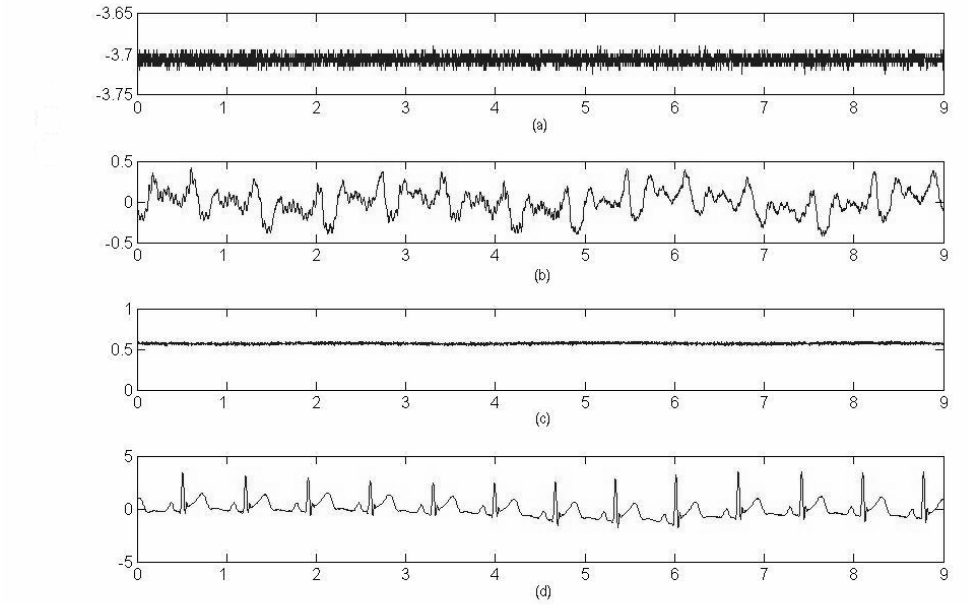

Fig. 5.28 Signals recorded from subject LV with HIC 2000 instrument using spot electrodes (a) *z(t)*, (b) *-dz/dt*, (c) Z_0, and (d) ECG (x axis: seconds, y axis: arbitrary unit).

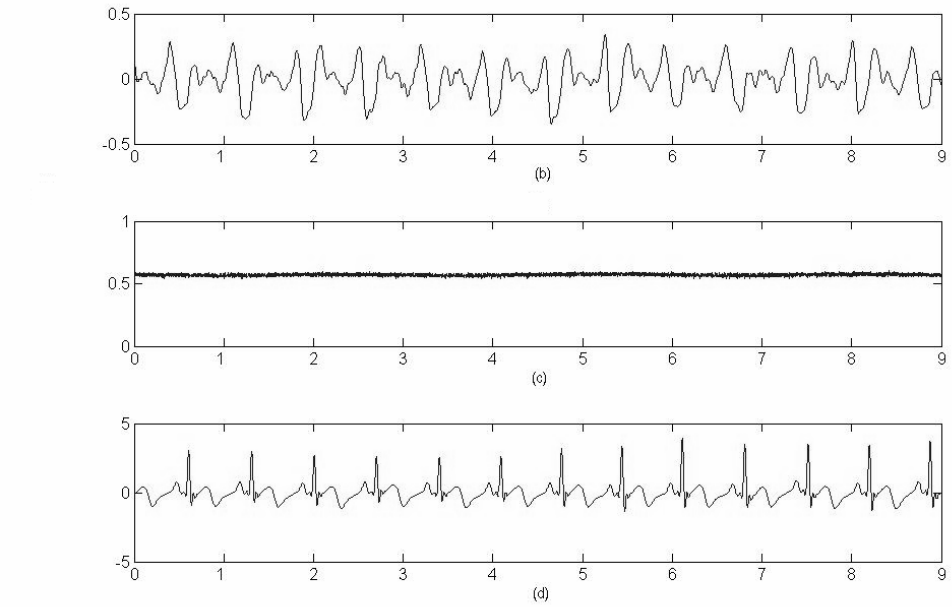

Fig. 5.29 Processed output of signal in Fig. 5.28 (b) -*dz/dt*, (c) Z_0, and (d) ECG (x axis: seconds, y axis: arbitrary unit).

Chapter 6
SUMMARY AND CONCLUSIONS

The project objectives involved developing

(a) a throx simulator for testing and calibration of impedance cardiograph hardware.

(b) an impedance cardiograph hardware.

Development of throx simulator involved upgrading the design of a microcontroller based circuit, by using a digital potentiometer based circuit to simulate step, sinusoidal, or other types of variation in change in the impedance. Thorax simulator was developed based on a design with digital potentiometer. An earlier design by Naidu [16] uses a microcontroller and analog switches based circuit to generate impedance variations, two input keys for selection of various options, and a LCD for display. The earlier design was capable of simulating only step change in impedance. In the new design, a digital potentiometer replaces the analog switches used to generate impedance variations. The digital potentiometer in the new design facilitates to simulate step, sinusoidal, or other types of variation in change in the impedance.

Development of impedance cardiograph involved improving the earlier design for better sensitivity by critically examining circuit blocks of an earlier developement hardware of impedance cardiography. The impedance cardiograph hardware consists of an excitation circuit, ICG extraction circuit, and ECG amplifier. The excitation circuit involves an oscillator as a source and a V/I converter with balanced ac coupling to drive the electrodes. The ICG extraction circuit consists of an instrumentation amplifier, AM demodulator, and base-line restoration circuit. The ECG amplifier has an instrumentation amplifier and a filter. A study on different oscillators was carried out in terms of short term amplitude stability and the most appropriate one was selected. The Wein bridge oscillator with modification in the

amplitude stabilization loop to improve its short term amplitude stability was selected as source with 100 kHz output. The high frequency current is injected through a high frequency transformer (PT6E) to provide galvanic isolation and impedance balanced output in order to minimize the external pick-up. In the ICG extraction circuit, a single chip instrumentation amplifier INA 128 was selected. The precision rectifier in the demodulator was redesigned for better performance. The parameters of the drift cancellation circuit have been modified for better performance. All the circuit blocks were tested together, and integrated on a single PCB with circuit layout designed with special consideration to reduce the noise pick-up.

The impedance cardiogram output from the instrument can be acquired in the PC through a data acquisition unit and can be further processed using MATLAB. ICG recordings were taken from normal male subject with band and spot electrodes.

It is suggested that an isolated power supply can be designed to make device portable and safe for clinical recordings. To ensure safty of the subject in which the recording will be carried out, optical isolation can be provided by using a linearized optoisolator between the outputs of the ICG instrument and the recording device.

Appendix A

Tracking based baseline restoration circuit for acquisition of bio signals

Vinod K. Pandey[1], Prem C. Pandey[2], and L. Venkatachalam[1]

[1]*BME Group, Bio School, IIT Bombay, Powai, Mumbai- 400 076, India*

[2]*EE Dept., IIT Bombay, Powai, Mumbai- 400 076, India*

Phone: (+91-22) 2576 7445

Fax: (+91-22) 2572 3707

E-mail: pcpandey@ee.iitb.ac.in

Abstract- Most of the bio signals have a baseline which may drift over a large range compared to the excursion of the signal of interest. To make effective use of the input dynamic range of the signal acquisition setup, this offset drift needs to be cancelled. The circuit reported here uses amplitude tracking technique for fast estimation and removal of the baseline drift. This circuit is independent of the processor to which the signal acquisition unit is interfaced, and can be used in set-ups with real-time as well as offline processing.

Keywords - Baseline restoration, Offset drift cancellation, Bio signal acquisition, Impedance cardiogram.

1. Introduction

Bio signals generally consist of a time-varying component, related to the physiological phenomenon of interest, superimposed on a baseline with an offset. This offset may drift over a range much larger than the excursion of the signal component. The baseline may be changing with time due to body movement and motion artifacts, or due to offset drift in the analog signal conditioning circuit. To make effective use of input dynamic range of the signal acquisition set-up, it is imperative to restore the baseline, at least partly, by removing the offset drift. Generally, the spectra of the drift are overlapped with that of the signal, making it difficult to restore the baseline drift by high pass filtering the signal. Here, we present a fast baseline restoration circuit, developed as a part of instrumentation for impedance cardiography, which may be used for acquisition of several bio signals.

Impedance cardiography is a noninvasive technique, based on sensing the variation in electrical impedance across the thorax, caused by change in the blood

volume during the cardiac cycle, for monitoring stroke volume and obtaining diagnostic information on cardiovascular functioning [2], [4], [5], [6], [8], [9], [10], [12]. The impedance change caused by cardiovascular activity is about 1 to 2 % of basal impedance [9, 10]. Sensing of this variation is confounded by variation in the thoracic impedance caused primarily by change in the dimension of the thoracic cage and/or skin-to-electrode impedance. These respiratory and motion artifacts have large amplitudes as compared to the impedance variation due to cardiovascular activity, and can cause a large baseline drift.

Several circuits for automated balancing of offset drift have been reported, including self-balancing system [3], successive approximation register (SAR) based method [10, 11], and integrator based drift cancellation system [4]. Self-balancing system circuit [3] requires up to $2n$ cycles for a n-bit D/A converter depending on the value of the offset. Successive approximation register (SAR) technique requires n clock cycles for a baseline balancing using n-bit SAR. A simpler version based on ramp approximation was later reported [4], which used an integrator in place of the SAR and D/A converter. However, capacitor discharge and op amp offset errors in the integrator introduce a drift, whose correction may lead to oscillatory drift. This can be removed in the subsequent signal processing, but it reduces the usable input dynamic range of A/D converter.

In the circuit presented here, tracking has been used, in place of successive approximation, for estimation and removal of the baseline drift. The baseline restoration requires only one clock cycle. This technique has been implemented using a microcontroller, and a D/A converter.

2. Method

The block diagram for the tracking based baseline restoration is shown in Fig. A.1. An estimate of the baseline voltage V_x is subtracted from the signal such that the signal after amplification would be within a range marked by two thresholds. It is to be noted that the baseline drift which does not result in crossing of a threshold range will not be compensated. This range is set after considering the excursion of the actual signal and the input range of the signal acquisition unit. Further, signal is not usable during the drift correction interval, and hence this time interval should be short and correction should not take place too frequently.

The up/down counter and a D/A converter are used to track the baseline drift in the input signal, and the estimated drift is subtracted from the input to give the drift balanced output V_o. Two thresholds [V_{t1}, V_{t2}] are selected corresponding to the desired range of the signal or the input range of the A/D converter used for signal acquisition. Whenever the output crosses the threshold range in either direction, a new estimation of the drift is carried out in the up/down counter depending on the direction of the drift, and the value is output to the D/A converter.

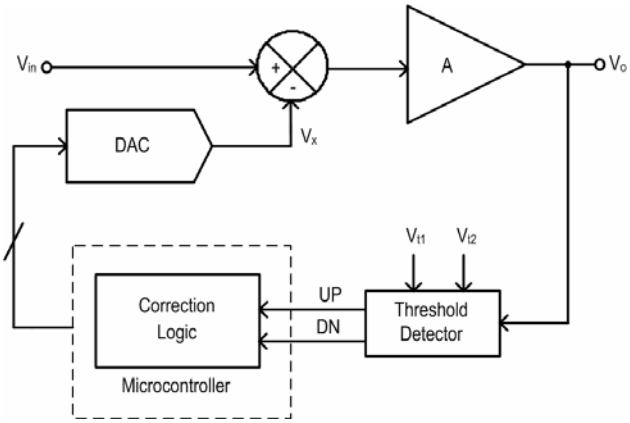

Fig. A.1 Block diagram for the tracking based baseline restoration

The baseline drift correction is done in one clock pulse, hence a relatively slower D/A converter can be used. One quantization step of the D/A converter after amplification is set to half of the output threshold range. Hence, after crossing of the threshold in either direction, the signal is brought back in the middle of the two thresholds.

The relationship between input voltage V_{in} and the output voltage V_o along with the correction voltage V_x is shown in Fig. A.2, for (a) increasing input and (b) decreasing input. It is to be noted that drift cancellation has a hysteresis, and the actual output depends on the direction of input change.

3. Circuit description

The circuit diagram of the microcontroller based implementation is shown in Fig. A.3. The circuit uses quad op amp TL084 as U1, 40-pin microcontroller AT89C52 [1] as U2, and 12-bit serial D/A converter TLV5618A as U3. The D/A converter has been used as 8-bit D/A converter by masking 4 LSBs. This circuit

has been developed for baseline drift removal in an impedance cardiograph [7] with ±5 V supply.

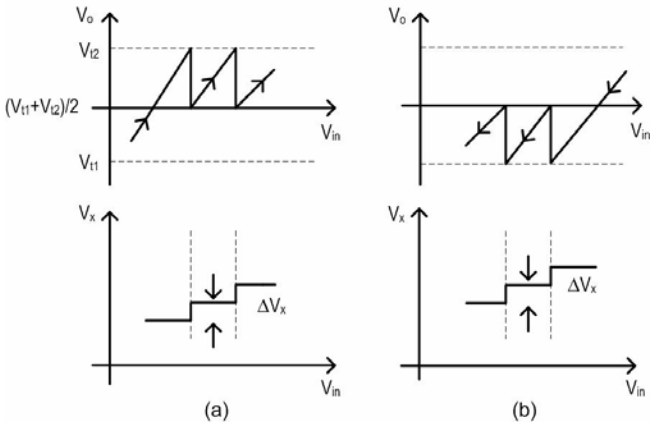

Fig. A.2 Input-output relationship for (a) increasing input, and (b) decreasing input.

Out of the four op amps in U1, op amp U1A is used as a summer for the input voltage, V_{in}, with gain A_s, the reference voltage, V_{REF}, with gain A_r, and the correction voltage, V_x, with gain $-A_x$. Hence the output is given as

$$V_o = V_{in}A_s + V_{REF}A_r - V_xA_x \qquad (1)$$

where, $A_s = (R_2 \,||\, R_3/(R_1 + R_2 \,||\, R_3))(1 + R_5/R_4)$,
$A_r = (R_1 \,||\, R_2/(R_3 + R_1 \,||\, R_2))(1 + R_5/R_4)$,
and $A_x = R_5/R_4$

Output of the D/A converter is unipolar, and hence reference voltage V_{REF} is required for realizing a bipolar range. Op amps U1B and U1C are used as comparators for comparing the output V_o with the threshold voltages V_{t1} and V_{t2}, which are set using a resistive divider. The port pins P1.0 and P1.1 of microcontroller U2 are used to scan threshold detector outputs. The tracking up/down counter of Fig. A.2 is realized using software inside the microcontroller. The count value is written as control byte to the D/A converter, interfaced serially to the microcontroller via serial peripheral interface (SPI). In our implementation, the microcontroller operates with 24 MHz crystal. The 8-bit up/down counter and SPI interface (3-wire) on port pins P3.0, P3.1, and P2.2 are implemented through software. The output voltage of the D/A converter can be varied from 0 to 4.2 V in 256 steps, in accordance with the counter output.

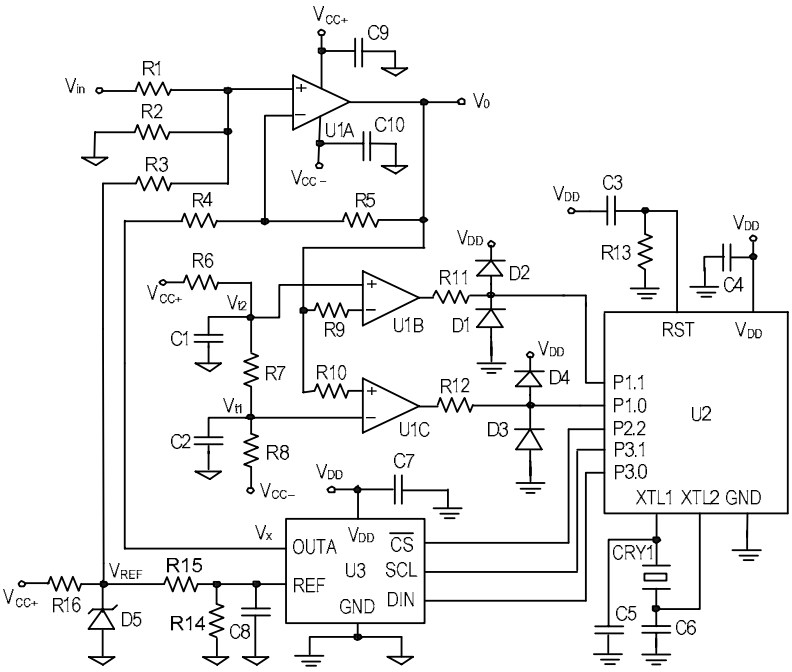

R1=R2=100 kΩ, R3=50 kΩ, R4=1 kΩ, R5=180 kΩ, R6=22 kΩ, R7=66 kΩ, R8=22 kΩ, R9=R10=R11=R12=10 kΩ, R13=15 kΩ, R14=R15=5.6 kΩ, R16=10 kΩ, C1=C2=10 nF, C3=10 µF, C4=0.1 µF, C5=C6=22 pF, C7=C8=C9=C10=0.1 µF, CRY1: 24 MHz Crystal, D1,D2,D3,D4: 1N4148, D5: 4.2 V Zener, V_{cc+}=+5 V, V_{cc-}=–5 V, V_{DD}=+5 V, U1: TL084, U2: AT89C52, U3: TLV5618A

Fig. A.3 Circuit diagram of the microcontroller based implementation.

A stable voltage references V_{REF} is obtained using Zener diode D5. An attenuated value of this is given as reference input to the D/A converter

$$V_{REF1} = [R_{14}/(R_{14}+R_{15})]/V_{REF} \quad (2)$$

Let input consist of actual signal V_s superimposed on baseline drift V_d.

$$V_{in} = V_s + V_d \quad (3)$$

Input range is mapped to the output voltage, and hence the gain for the input signal is selected as

$$A_s = (V_{t2} - V_{t1})/(V_{s\max} - V_{s\min}) \quad (4)$$

If the summer output V_o goes below the lower threshold V_{t1}, the comparator U1C is driven to positive saturation, producing high input to pin P1.0 of microcontroller U2. The up/down counter is decremented, and the D/A converter output V_x is correspondingly decremented by one step. Similarly, if V_o goes above the upper threshold V_{t2}, input P1.1 of microcontroller becomes high, the counter is incremented and V_x is increased by one step. Thus the correction voltage V_x is given as

$$V_x(t_n+1) = \begin{cases} V_x(t_n)+\Delta V_x, & V_o(t_n) > V_{t2} \\ V_x(t_n)-\Delta V_x, & V_o(t_n) < V_{t1} \\ V_x(t_n), \text{ otherwise.} \end{cases} \quad (5)$$

For N steps in the D/A converter, the step voltage is given as

$$\Delta V_x = (V_{s\max} - V_{s\min}) / N \quad (6)$$

The gain for the correction voltage is given as

$$A_x = 0.5(V_{t2} - V_{t1}) / \Delta V_x \quad (7)$$

This feedback voltage is used for baseline drift correction to bring V_o within the threshold range. If V_o is still outside the range [V_{t1}, V_{t2}], the process is repeated. If the output V_o is within the range [V_{t1}, V_{t2}], both the comparator outputs are low, the count in the counter is not changed, the correction voltage remains constant.

3. Results

Component values shown in Fig. A.3 were selected for threshold voltages of ±3 V, signal gain of 45, correction voltage gain of 180, V_{REF} = 4.2 V, and reference voltage gain of 90. The maximum time for restoring the drift is less then 1 ms. An example of drift cancellation by the implemented circuit is shown in Fig. A.4. Input consist of 40 mV (p-p) impedance cardiogram waveform, with fundamental frequency of 1.2 Hz, superimposed on a slow varying baseline drift, with a slope of 40 mV/s. Output waveform shows that baseline has been restored and drift is tracked when the signal after amplification crosses the threshold range in either direction.

4. Conclusion

A tracking based circuit for fast restoration of baseline by canceling offset drift has been presented. The correction logic is implemented in software with an 8-bit microcontroller. Although the circuit has been developed for impedance cardiography, it can be used for acquisition of other bio signals with large drift or abrupt baseline shift. This circuit is independent of the processor to which the signal acquisition unit is interfaced and can be used in set-ups with real time as well as offline processing. In the present implementation, tracking of baseline is initiated by the output going out of the defined range.

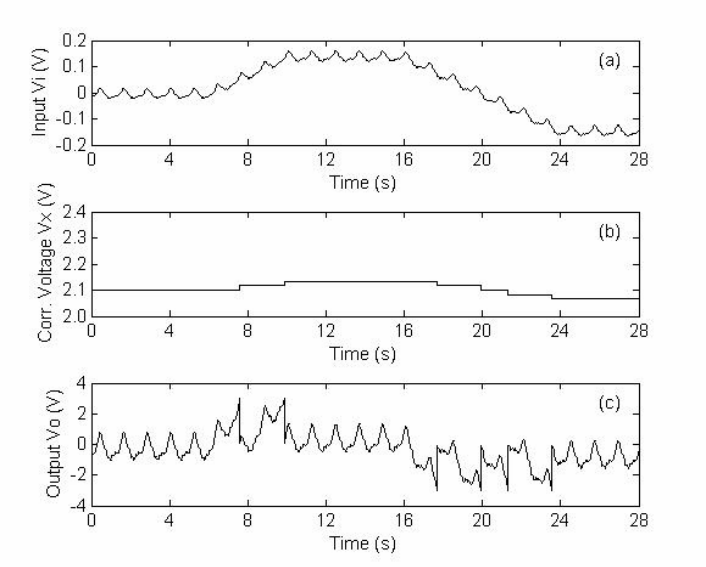

Fig. A. 4 Output of the baseline restoration circuit for the impedance cardiogram with large baseline shifts (a) input, (b) correction voltage, (c) output.

Alternatively, the microcontroller can be programmed to carry out the tracking for drift cancellation at periodic intervals, which may be appropriate for certain applications.

References

1. AT89 Series Microcontroller Data Book (1997), Atmel Corp., San Jose, California.
2. Baker LE (1989), Principle of the impedance technique, IEEE Eng Med Biol Mag, 8: 11-15.
3. Cohen A, Longini RL (1971), Self-balancing system for medical and physiological instrumentation, IEEE Trans Biomed Eng, 18:66–69.
4. Joshi SM, Pandey PC (1994), A cardiac output monitor using impedance plethysmography, Proc Int Conf on Recent Advances in Biomedical Eng, Hyderabad, India, 157–160.
5. Kubicek WG, Kottke FJ, Ramos MU, Patterson RP, Witsor DA, Labree JW, Remole W, Layman TE, Schoening H, Garamela JT (1974), The Minnesota impedance cardiograph-theory and application, Biomed Eng, 9:410–416.
6. Kubicek WG, Kinnen E, Paterson RP, Witsoe DA (1967), Impedance plethysmograph, U. S. Patent No. 3,340,867.
7. Manigandan NS (2004), Development of hardware for impedance cardiography, M. Tech. thesis (unpublished), Biomedical Eng Group, IIT Bombay, Mumbai, India.
8. Nyboer J (1970), Electrical Impedance Plethysmography, Charles C. Thomas, Springfield, Massachuates.

9. Patterson R.P (1989), Fundamentals of impedance cardiography, IEEE Eng Med Biol Mag, 8: 35–38.
10. Qu M, Zhang Y, Webster JG, Tompkins WJ (1986), Motion artifacts from spot and band electrodes during impedance cardiography, IEEE Trans Biomed Eng, 33: 1029–1036.
11. Shankar TMR, Webster JG (1984), Design of an automatically balancing electrical impedance plethysmograph, J Clin Eng, 9:129–134.
12. Sramek BB (1994), Thoracic electrical bioimpedance: Basic principles and physiologic relationship, Noninvas Cardiol, 3:83–88.

Appendix B

LIST OF COMPONENTS

Table B-1: List of components for thorax simulator

Component designator	Part description	Component specification	Qty.	Approx. Rate (Rs.)	Approx cost (Rs.)
R1,R3,R22,R27	Resistor	220 Ω, 1/4 Watt	4	0.50	2.00
R2,R17,R24	Resistor	2.2 kΩ, 1/4 Watt	3	0.50	1.50
R8,R4	Resistor	4.7 kΩ, 1/4 Watt	2	0.50	1.00
R5,R16	Resistor	10 Ω, 1/4 Watt	2	0.50	1.00
R6,R20	Resistor	47 Ω, 1/4 Watt	2	0.50	1.00
R7,R13	Resistor	100 Ω, 1/4 Watt	2	0.50	1.00
R9,R14,R15,R21	Resistor	10 kΩ, 1/4 Watt	4	0.50	2.00
R10	Resistor	330 Ω, 1/4 Watt	1	0.50	0.50
R11,R12,R18,R19, R25,R28,R29,R30, R31,R32	Resistor	33 kΩ, 1/4 Watt	6	0.50	3.00
R23	Resistor	100 kΩ, 1/4 Watt	1	0.50	0.50
R26	Resistor	11 kΩ, 1/4 Watt	1	0.50	0.50
C1,C2,C3,C4,C5,C6, C7,C8,C9,C10,C11, C12,C13,C14	Ceramic capacitor	0.1 µF	14	0.50	7.00
D1	Voltage reference	LM385-2.5	1	1.00	1.00
Y1	Crystal oscillator	20 MHz	1	5.00	5.00
S1	Switch	SPDT	1	8.00	8.00
S2, S3	Soft keys		2	10.00	20.00
U1,U6	IC	LM7805	2	10.00	20.00
U3	IC	AD5290	1	100.00	50.00
U2	IC	LM324	1	10.00	10.00
U4,U5,U8,U9	IC	CD4066	4	9.00	36.00
U7	IC	PIC18F252	1	200.00	200.00
Battery		9 V	1	10.00	10.00
JP1 - JP5	2-pin male connector		5	1.50	7.50
J1	16 character by two line LCD		1	150.00	150.00
PCB			1	500.00	500.00
		Total cost			1038.50

Table B-2: List of components for ICG instrument

Component designator	Part description	Component specification	Qty	Approx. Rate (Rs.)	Approx. cost (Rs.)
R1,R3	Resistor	1.5 kΩ, 1/4 Watt	2	0.50	1.00
R2,R14,R16,R32	Resistor	0 Ω, 1/4 Watt	4	0.50	2.00
R4	Resistor	6.4 kΩ, 1/4 Watt	1	0.50	0.50
R5	Resistor	750 Ω, 1/4 Watt	1	0.50	0.50
R6,R43,R53,R60, R67,R72	Resistor	1 kΩ, 1/4 Watt	6	0.50	3.00
R7,R8,R13,R20,R21 ,R24,R25,R26,R30, R33,R35,R36,R39, R49,R66,R73,R74	Resistor	10 kΩ, 1/4 Watt	17	0.50	8.50
R9	Resistor	3.3 kΩ, 1/4 Watt	1	0.50	0.50
R10	Resistor	4.9 kΩ, 1/4 Watt	1	0.50	0.50
R11,R17,R18,R22, R23,R46,R51,R62, R63,R64,R65	Resistor	100 kΩ, 1/4 Watt	11	0.50	5.50
R15,R12	Resistor	47 kΩ, 1/4 Watt	2	0.50	1.00
R27,R57	Resistor	27 kΩ, 1/4 Watt	2	0.50	1.00
R28,R58	Resistor	5.2 kΩ, 1/4 Watt	2	0.50	1.00
R31,R34	Resistor	500 Ω, 1/4 Watt	2	0.50	1.00
R37	Resistor	3.9 kΩ, 1/4 Watt	1	0.50	0.50
R38,R40,R50,R61	Resistor	100 Ω, 1/4 Watt	4	0.50	2.00
R52,R42	Resistor	1 MΩ, 1/4 Watt	2	0.50	1.00
R45	Resistor	12 kΩ, 1/4 Watt	1	0.50	0.50
R47	Resistor	33 kΩ, 1/4 Watt	1	0.50	0.50
R48	Resistor	82 kΩ, 1/4 Watt	1	0.50	0.50
R54,R75	Resistor	15 kΩ, 1/4 Watt	2	0.50	1.00
R55	Resistor	220 kΩ, 1/4 Watt	1	0.50	0.50
R56	Resistor	3.3 MΩ, 1/4 Watt	1	0.50	0.50
R59	Resistor	180 kΩ, 1/4 Watt	1	0.50	0.50
R68,R70,R71	Resistor	5.6 kΩ, 1/4 Watt	3	0.50	1.50
R69	Resistor	8.2 kΩ, 1/4 Watt	1	0.50	0.50
C1,C2	Ceramic capacitor	1 nF	2	0.50	1.00
C3,C4,C5,C6,C7,C8, C12,C13,C14,C15, C16,C17,C20,C21, C23,C26,C27,C29, C31,C32,C33,C34, C35,C36,C37,C41,	Ceramic capacitor	0.1 uF	48	0.50	24.00

C43,C44,C45,C46, C48,C49,C51,C52, C53,C54,C56,C57, C60,C61,C62,C63, C64,C65,C66,C69, C72,C73					
C9,C10,C25	Ceramic capacitor	47 uF	3	0.50	1.50
C11,C18,C19,C67, C68,C70	Ceramic capacitor	10 nF	6	0.50	3.00
C22,C24,C38,C55, C58	Ceramic capacitor	33 nF	5	0.50	2.50
C28,C30,C39,C40, C47,C50, C75	Ceramic capacitor	10 uF	7	0.50	3.50
C42	Ceramic capacitor	100 pF	1	0.50	0.50
C59	Ceramic capacitor	2.2 nF	1	0.50	0.50
C71,C74	Ceramic capacitor	22 pF	2	0.50	1.00
D1,D2,D3,D4,D6, D7,D8,D9, D11	Diode	1N4148	8	0.50	4.00
D5,D10	Voltage reference	LM385-2.5	2	10.00	20.00
S1	Switch	SPDT	1	8.00	8.00
U1 – U7, U10 – U14, U18 – U23, U26	IC	LF357	19	35.00	665.00
U8,U17	IC	INA128	2	100.00	200.00
U9,U16	IC	LM7805	2	10.00	20.00
U15	IC	LM7905	1	10.00	10.00
U24	IC	AT89C52	1	200.00	200.00
U25	IC	TLV5618A	1	50.00	50.00
T1	Pulse Transformer	PT6E	1	700.00	700.00
Q1	FET	BFW10	1	5.00	5.00
J1 – J9	2-pin male connector		9	1.50	13.50
JP1 – JP17	2-pin male connector		17	0.50	8.50
Y1	Crystal oscillator	24 MHz	1	5.00	5.00
PCB			1	500.00	500.00
		Total cost			2464.00

Appendix C

PCB LAYOUT

Impedance cardiograph:

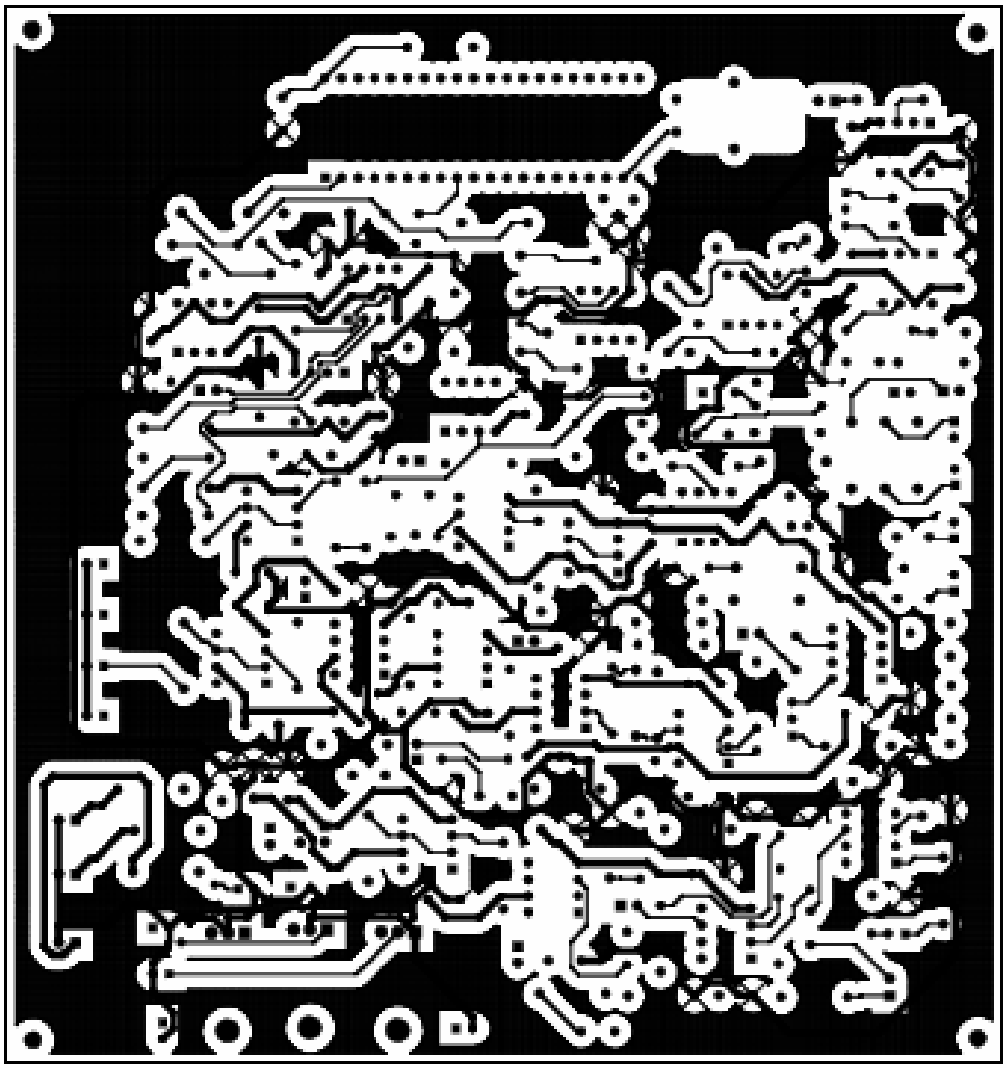

Fig C.1 Component side of impedance cardiograph PCB

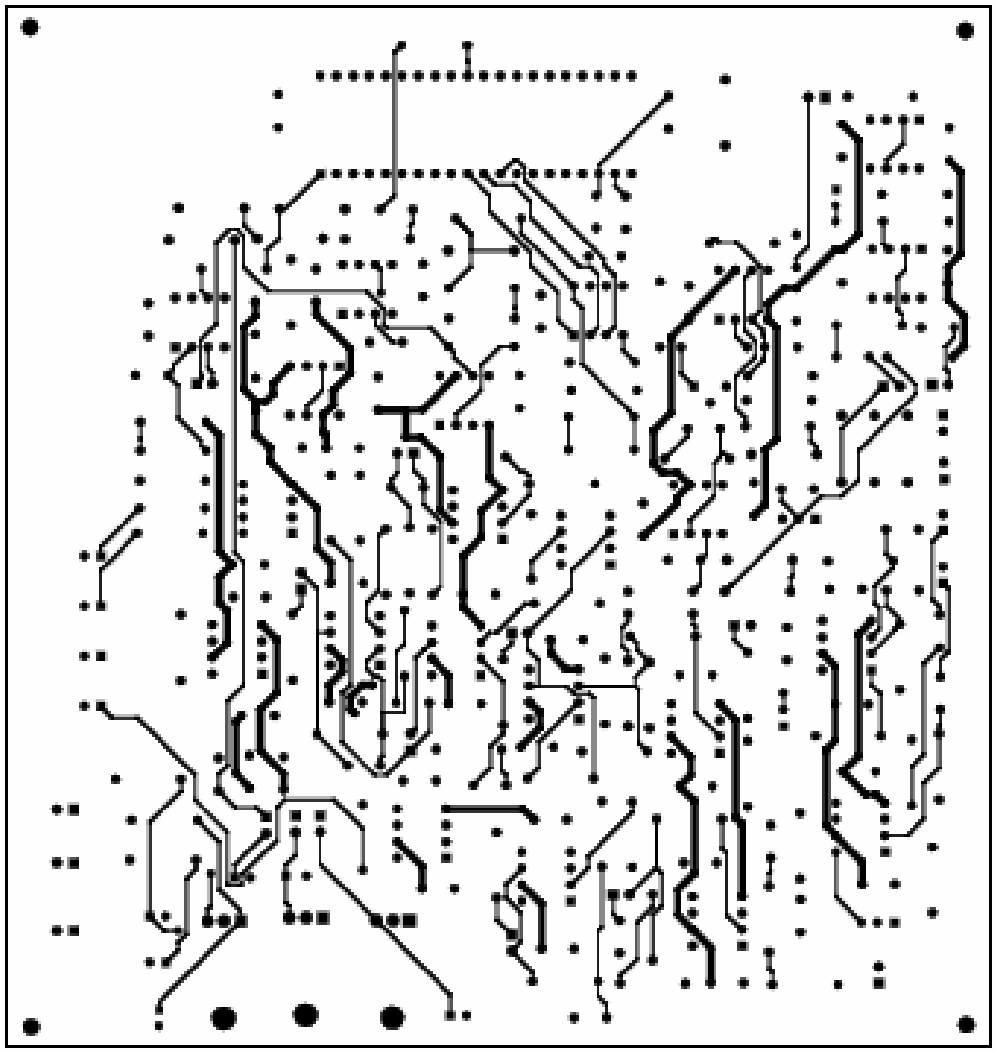

Fig C.2 Solder side of impedance cardiograph PCB

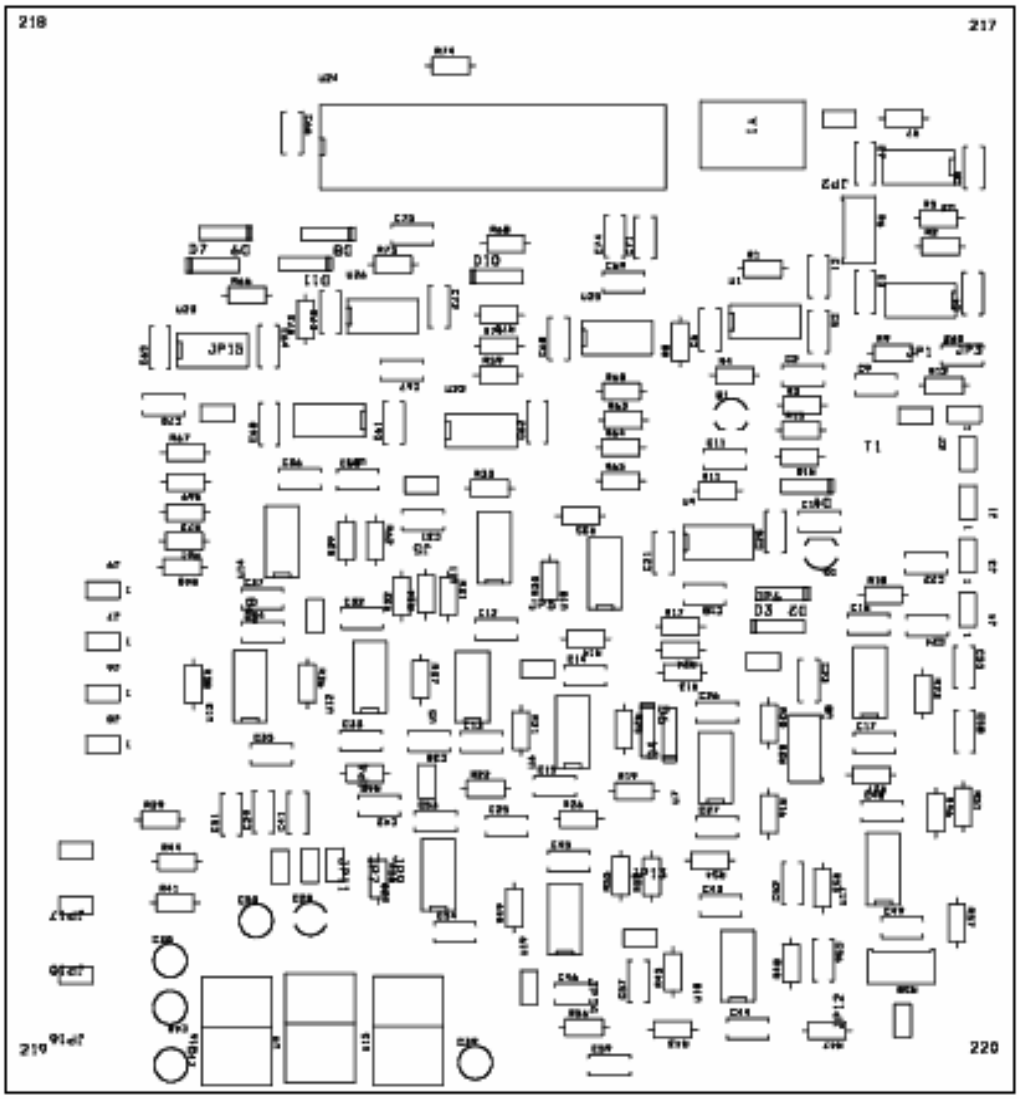

Fig C.3 Component layout of impedance cardiograph PCB

Thoracic impedance simulator:

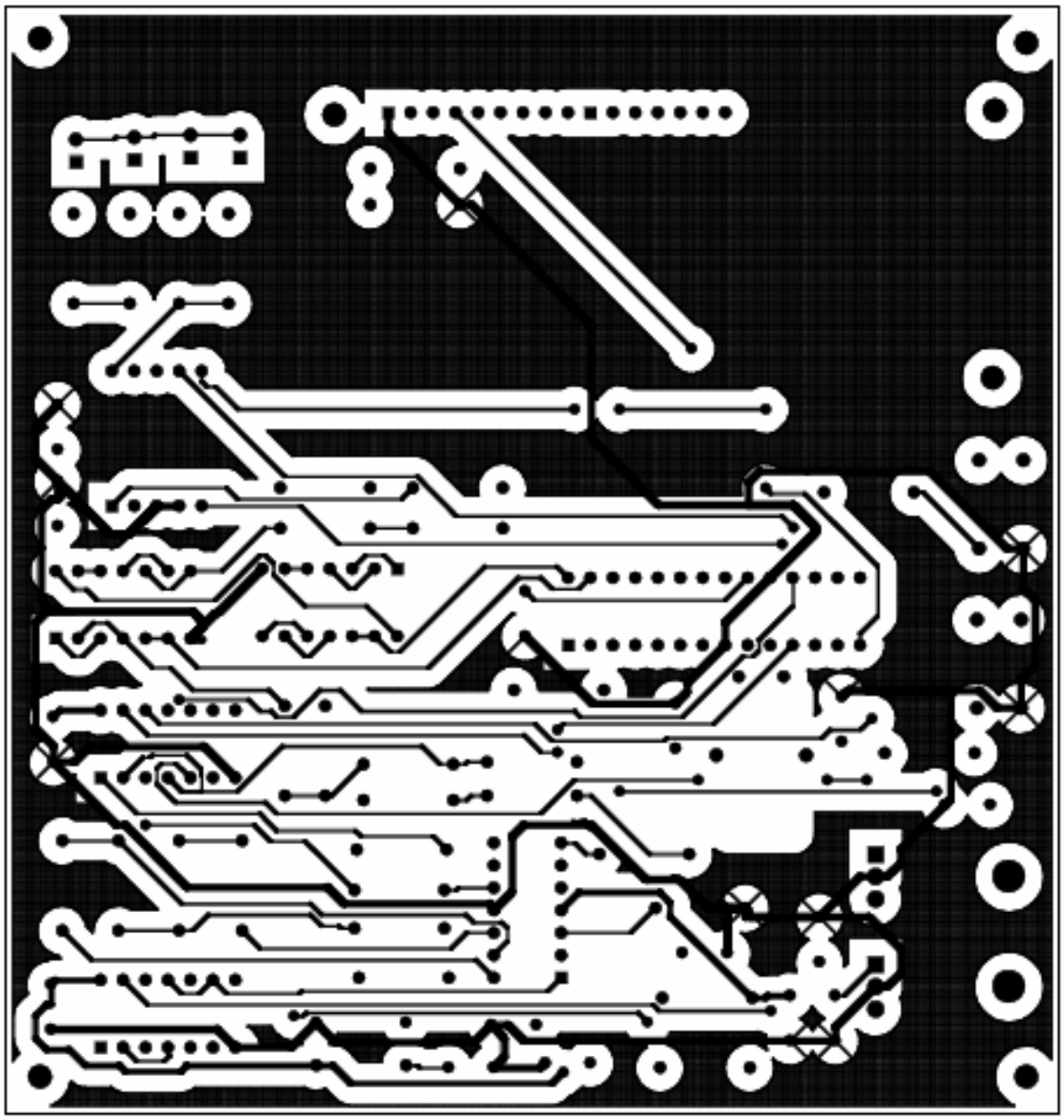

Fig C.4 Component side layout of simulator PCB

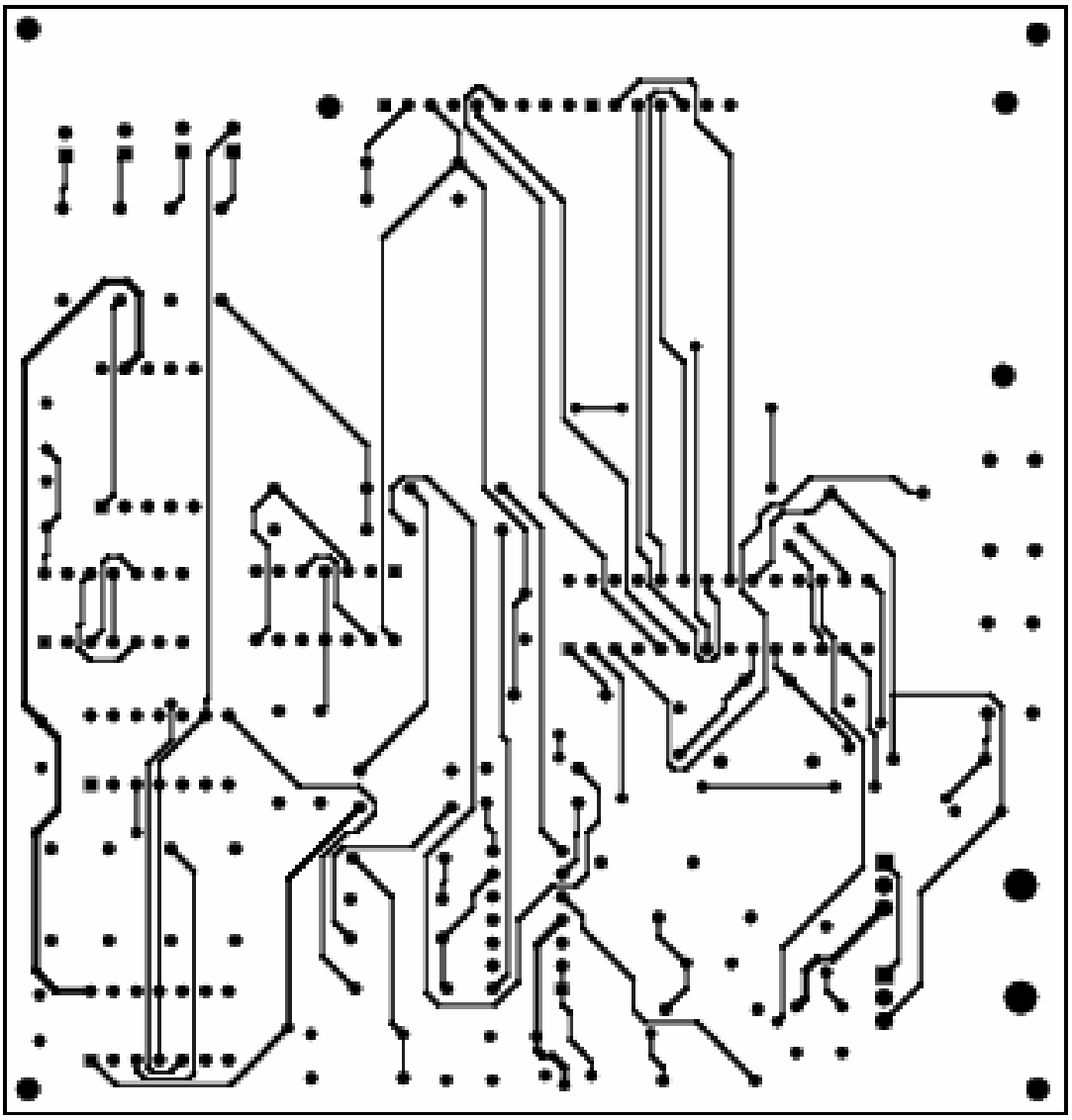

Fig C.5 Solder side layout of simulator PCB

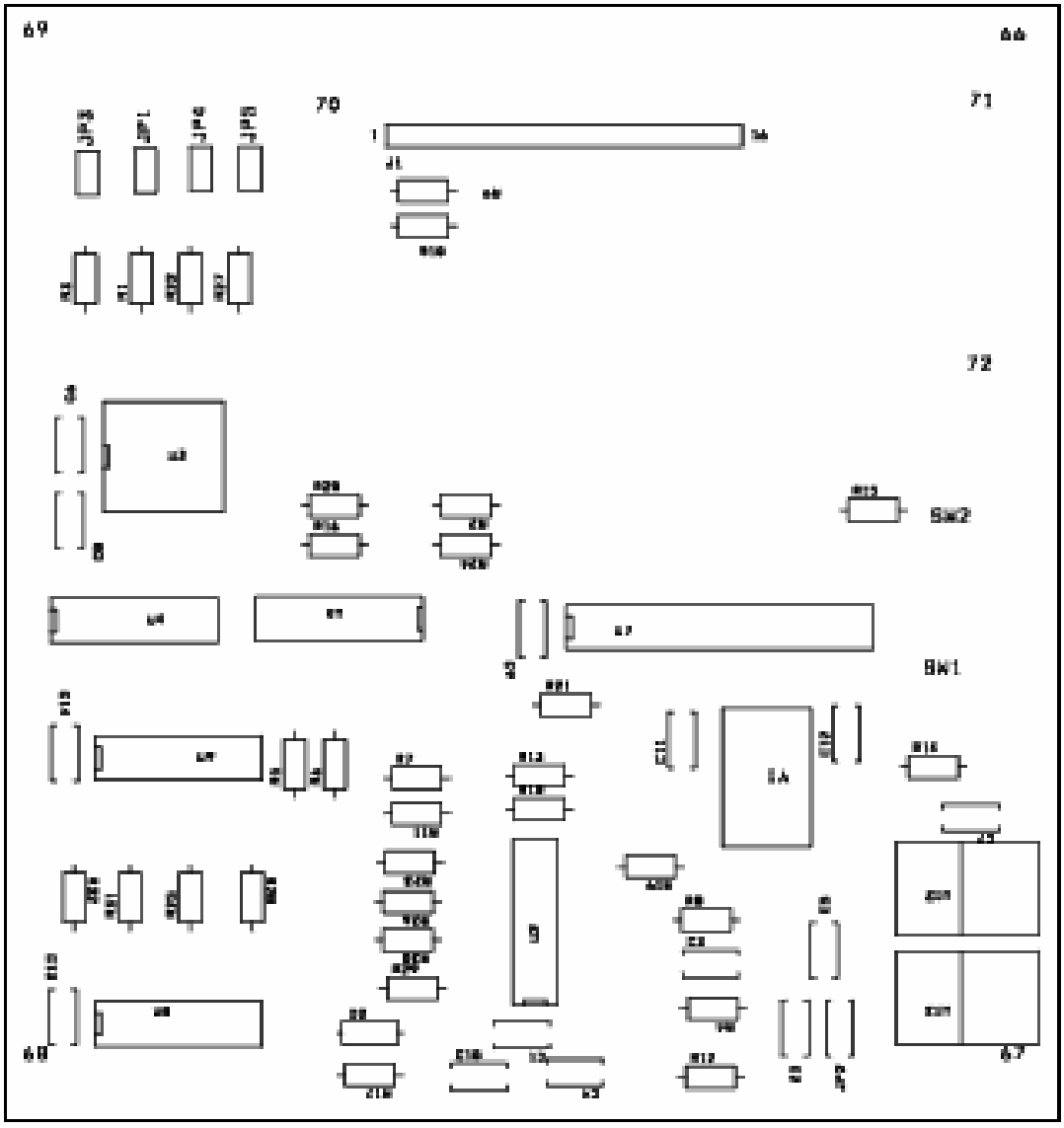

Fig C.6 Component placement layout of simulator PCB

REFERENCES

[1] A. C. Guyton, *Textbook of Medical Physiology*. 7th ed., Philadelphia: Saunders, 1986.

[2] W. F. Ganong, *Review of Medical Physiology*, 13th ed., Connecticut: Prentice-Hall, 1987.

[3] "Cardiothoracic surgery," Keck School of Medicine of University of Southern California, http://www.cts.usc.edu/graphics/heart-crosssection1.jpg, downloaded on 17th July 2003.

[4] L. E. Baker, "Principles of the impedance technique," *IEEE Eng. Med. Biol. Mag.*, vol.8, pp. 11-15, Mar. 1989.

[5] R. P. Patterson, "Fundamentals of impedance cardiography," *IEEE Eng. Med. Biol. Mag.*, pp. 35-38, Mar. 1989.

[6] A. K. Deshpande, G. D. Jindal, P. M. Jagasia, K. V. S. Murali, P. A. Bharadwaj, K. I. Tahilkar, and G. B. Parulkar, "Impedance plethysmography of thoracic region: impedance cardiography," *J. Post. Med.*, vol. 36, No. 4, pp. 207–212, 1990.

[7] J. Malmivuo and R. Plonsey, "Impedance plethysmography," in *Bioelectromagnetism*, 2nd ed., New York: Oxford Univ. Press, 1995.

[8] W. G. Kubicek, F. J. Kottke, and M. U. Ramos, "The Minnesota impedance cardiograph – theory and applications," *Biomed. Eng.*, vol. 9, pp. 410-416, Sept. 1974.

[9] B. B. Sramek, "Thoracic electrical bioimpedance: basic principle and physiologic relationship," *Noninvas. Cardiol.*, vol. 3, pp. 83-84, 1994.

[10] J. Vedru, "Electrical impedance methods for the measurement of stroke volume in man: state of art," *Acta et comm.*, Univ. Tartuensis, Tartu, Estonia, pp. 110-129, 1994.

[11] S. M. Joshi / P. C. Pandey (supervisor): "A cardiac output monitor," *B.Tech. Project report*, EE Dept., IIT Bombay, 1993.

[12] S. M. Joshi and P. C. Pandey, "A cardiac output monitor using impedance plethysmography," in Proc. *Int. Conf. Rec. Adv. Biomed. Eng.*, (Osmania Univ. Hyderabad, India), pp. 157-160, Jan. 1994.

[13] K. S. Patwardhan / P. C. Pandey (supervisor): "An impedance cardiograph for stress testing," *M.*Tech. Dissertation, EE Dept., IIT Bombay, 1997.

[14] B. Kuriakose / P. C. Pandey (supervisor): "An impedance cardiograph," *M.Tech. Dissertation*, BME Group, IIT Bombay, 2000.

[15] N. S. Manigandan / P. C. Pandey (supervisor): "Development of hardware for impedance cardiography," *M.Tech. Dissertation*, BME Group, IIT Bombay, 2004.

[16] N. K. S. Naidu / P. C. Pandey (supervisor): "Hardware for impedance cardiography," *M.Tech. Dissertation*, BME Group, IIT Bombay, 2005.

[17] V. K. Pandey / P. C. Pandey (supervisor): "Signal processing for impedance cardiography," *Ph.D. 2nd Progress Seminar Report*, BME Group, IIT Bombay, 2004.

[18] V. K. Pandey and P. C. Pandey, "Cancellation of respiratory artifact in impedance cardiography," in Proc. *27th Annual Int. Conf. of the IEEE Eng. Med. Biol. Soc.* (IEEE/ EMBC'05), Shanghai, China, Sept. 1-4, 2005.

[19] Y. Zhang, M. Qu., J. G. Webster, W. J. Tompkins, B. A. Ward, and D. R. Bassett, "Cardiac output monitoring by impedance cardiography during treadmill exercise," *IEEE Trans. Biomed. Eng.*, vol. 33, pp. 1029-1041, Nov. 1986.

[20] M. Qu, Y. Zhang, J. G. Webster, and W. J. Tompkins, "Motion artifact from spot and band electrodes during impedance cardiography," *IEEE Trans. Biomed. Eng.*, vol. 33, pp. 1029-1036, Nov. 1986.

[21] F. R. Dungan, *Op Amps & Linear Integrated Circuits for Technicians*, 2nd ed., New York: Delmar, 1992.

[22] J. M. Fiore, *Op Amps and Linear Integrated Circuits*, New York: Delmar, 2001.

[23] J. G. Webster, *Medical Instrumentation-Application and Design*, 3rd ed., New Delhi: John Wiley, 1998.

[24] P. W. Van der Walt, "A Wein-bridge oscillator with high-amplitude stability," *IEEE Trans. Instrum. Meas.*, vol. 30, pp. 292-294, 1981.

[25] E. Oxner, *Designing with Field Effect Transistors*, 2nd ed., New York: McGraw-Hill, 1990.

[26] J. N. Sarvaiya / P. C. Pandey (supervisor): "Development of an Impedance Glottograph," *M.Tech. Dissertation*, BME Group, IIT Bombay, 2006.

[27] J. Milman, *Microelectronics:Digital and Analog Circuits and Systems*, New York: McGraw-Hill, 1979.

[28] "HIC-2000 and HIC-3000 Product Information", Bio-Impedance Technology (Connecticut, U.S.A.), Available online, http://www.microtronics-nc.com/BIT/HICProductInfo.html, downloaded on 10th August 2006.